# Detectors and Data Analysis Techniques for Wide Field Optical Imaging

**By M.J.Irwin**

Royal Greenwich Observatory, Madingley Road, Cambridge, CB3 0EZ, UK

This contribution reviews the current status of optical wide field survey astronomy and the basic techniques that have been developed to capitalise on the large volumes of data generated by modern optical survey instruments. Topics covered include telescope design constraints on wide field imaging; the properties of CCD detectors and wide field CCD mosaic cameras; preprocessing CCD data and combining independent digitised frames; opitmal detection of images and digital image centering and photometry methods. Although the emphasis is geared toward optical imaging problems, most of the techniques reviewed are applicable to any large format two-dimensional astronomical image data.

---

## 1. Wide Field Survey Astronomy

### 1.1. *Background*

Astronomy is basically an observational science, rather than an experimental one, and the development and advancement of the subject has relied heavily on surveys of the sky at optical wavelengths to expand our knowledge of the observable Universe. Surveys form a basic foundation of observational astronomy, and provide three generic types of information:

- quantitative statistical information on the distribution of objects in our own galaxy and the Universe
- the ability to discover radically new types of object
- the means of selecting representative samples of certain types of (rare) objects, particularly the brightest examples, for further study with large telescopes.

Statistical surveys are beginning to rely ever more heavily on the wide field multi-object fibre spectroscopy capabilities of large telescopes, described elsewhere in this volume. However, surveying for rare objects, or even discovering new categories of objects, is more problematic, since often their surface densities on the sky are sufficiently low to render fibre spectroscopy approaches grossly inefficient.

We can investigate the problems in surveying for rare types of object and estimate the chances of discovering new classes of object by borrowing a statistical analogy from biological systems (Thejll & Shipman 1988). In studies of the diversity of a population of butterflies, Fisher, Corbett & Williams (1943) proposed a simple relationship linking the sample size, $N$ and the number of species present, $S$, such that

$$S = A \times ln(1 + N/A) \tag{1.1}$$

where $A$ the diversity index, parameterises the tendency of the population to produce separate sub-species. Although, the formula is necessarily a simplification of a complex classification process, Fisher *et al.* argued that for any procedural sub-classification scheme based on combining distinguishing factors multiplicatively, a logarithmic series provides a good practical approximation. In particular, if a similar survey has already been done, the above formula enables the diversity parameter $A$ to be derived and sub-

sequently used in predicting how many further observations are likely to be needed in order to, for example, find one new species.

As an example Thujll and Shipman (1988) applied this method to the Palomar– Green UVX survey covering some 10,000 deg$^2$ of Northern sky to B= 16 and find

$S = 11; N = 1550; \Rightarrow A = 1.6$ – stellar and

$S = 6; N = 165; \Rightarrow A = 1.2$ – non–stellar

where the categories included the first gravitational lens, ultrahot stars and new type of variables. Demers *et al.* (1986) are undertaking a similar UVX survey in the Southern sky and figure 1 illustrates how application of the Fisher *et al.* formula leads to a prediction of how much detailed followup of candidates is required to find one or more new species. Selecting candidates in a UVX survey is relatively straightforward and cheap in terms of telescope time. On the other hand spectroscopic followup of individual objects is a relatively costly exercise and the Fisher *et al.* formula enable researchers to assess how much telescope time is likely to be needed to reach some defined goal.

Naturally, simply looking at more objects is not the only way to find new species or find more examples of rare objects as the following points emphasise:

- Increasing N exponentially usually $\Rightarrow$ more sky coverage; this can be a problem at bright magnitudes.
- Alternatives are to survey in new wavebands, particularly outside the wavelength range normally sampled.
- Survey at different epochs, ie. time series sampling, which can give orthogonal information to conventional spectroscopy or broad-band wavelength coverage.
- Survey to fainter levels and potentially sample a different spatial volume, eg. larger look-back time for a cosmological sample.
- Higher accuracy measurements enable 'normal' object locii to be better defined, hence the parameter phase space volume for unusual objects is increased and they are easier to delineate.

### 1.2. *General Survey Constraints*

It is well known that reliable quantitative surveys form a vital constituent in the future success of any large telescope programme, just as the surveys based on photographic plates taken with the Palomar Schmidt and UK Schmidt have been vital to the success of the present generation of large (ie. 4m class) telescopes. Survey instruments and their associated followup facilities must however be well matched. As an example, consider the current surveys on 1.2m Schmidt telescopes which reach limiting magnitudes equivalent to $V = 21 - 22$ in 1 hour exposures. These are well matched to followup spectroscopy on 4m-class telescopes, where $\sim 5$Å resolution spectra at $V = 21 - 22$ take of order 1 hour exposure time. The 'natural' survey time on these Schmidt telescopes is approximately 1 hour since that is when most exposures are limited by sky noise rather than emulsion/fog noise. To go 1 magnitude fainter than a sky-limited plate would require an impractical $\times$ 6.25 increase in exposure. Contrast this with the equivalent numbers for a modern CCD on a 2–3m class telescope, where the limiting magnitudes would be $V = 24 - 25$ in a 10–15 minute "natural" survey time exposure. Clearly, to do spectroscopic followup of objects detected near the limit of these types of CCD survey will require at least 8m-class telescopes. Yet without suitably deep survey material, where are the input targets for 8m-class telescopes going to come from ?

Although the importance of next generation survey work is self-evident, it is only relatively recently that practical work has been initiated to develop survey instruments beyond the Palomar and UK Schmidt photographic surveys. The competitiveness of

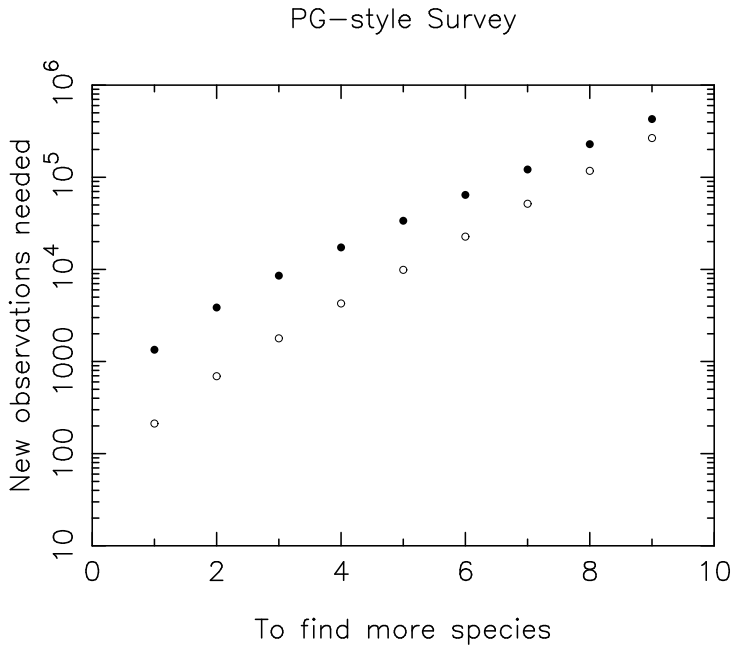


FIGURE 1. The Fisher *et al.* formula applied to the Palomar–Green survey; open symbols galaxies, filled symbols stars. Note that to significantly increase the number of new types of object found requires an exponential increase in the number of observations.

---

the very large telescope programmes in fundamental areas of research such as large scale structure and the formation and evolution of galaxies and AGN, critically depends on the quality of the survey work. We cannot efficiently run 8-16m telescopes in the next decade if we do not have at the same time proper survey facilities with which to select the best objects to follow-up. Fortunately, CCD mosaic cameras are now becoming available and are becoming competitive with traditional photographic survey methods. This provides a good excuse to examine the current wide field survey capabilities in optical astronomy and to assess the requirements for future optical survey material.

### 1.3. *Current Situation of Optical Sky Surveys*

Despite the considerable advances of detector technology within astronomy very little improvement has been made in surveys beyond those available in the 1950's when the Palomar Sky Survey was carried out. A photographic plate taken on a 1.2m Schmidt is sky limited in about 1 hour, covers an area, $A$, on sky of some 40 square degrees, but is only $\approx 2\%$ efficient, $\eta$. We can characterise the overall effectiveness of the system by the product of efficiency and area covered. For photographic plates, $\eta \times A \approx 0.5$. The current best sky surveys therefore amount to no more that a 120 second glance of the Universe and all the recent dramatic improvement in exploiting the exisiting survey material is due entirely to the advent of the fast automatic plate measuring machines (for a review see Lasker, 1995a). By routinely processing the $\sim$ 4Gbytes of information on a Schmidt plate in a matter of a few hours, these machines have opened up new areas of

quantitative survey astronomy. However, the planned and current photographic surveys (UKST second epoch R and new Palomar Sky Survey eg. Morgan, 1995) will not provide a significant improvement in this situation since essentially they will be extending what already exists.

Because of the low efficiency and relatively high grain noise of photographic plates, sky-limited exposures produce typical limiting magnitudes of 21 in the red and 22–23 in the blue. Intrinsic photometric errors are in the range $0.05 - 0.^m1$ for objects a magnitude or more above the plate limit, with the equivalent astrometric errors around $1\mu$, or $\sim$0.1 arcsec. Systematic photometric and astrometric field errors are also present. Photometric field errors up to $0.^m25$ are not uncommon, though with careful processing the photometric errors can generally be reduced down to the level of the random errors. Astrometrically, global distortions (some magnitude-dependent and some not *e.g.* Irwin, 1994) of up to 1 arcsec also affect plates. Again with careful processing and effective use of astrometric standards, most of these systematic errors can be reduced to the level of better than 0.25 arcsec over 2 degree scale sizes (the requirement for the 2DF facility on the AAT), and to less than the individual object random errors over the field sizes for spectroscopy on normal telescopes (*e.g.* . for blindoffsetting targets onto slits to 0.1 arcsec accuracy).

Impressive though these figures are for all sky surveys, they are unlikely to improve dramatically due to the relatively poor dynamic range of photographic detectors (Irwin (1992). Even the recent innovative use of 4415 emulsion by the UKST (Russell *et al.* , 1992; Parker *et al.* , 1994) will not significantly change this situation. The current generation of measuring machines, including those nearing completion, fully exploit the present and planned photographic sky surveys. In order to make a significant advance (say a factor of 10) over current material any new survey must be based on detectors that are essentially photon noise limited, such as CCDs.

One area where Schmidt survey work leads the way for future CCD surveys lies in the already developed ability to handle large volumes of data. For example, the high latitude sky in the Northern hemishere covers some 10,000 deg$^2$. If sampled at 0.4 arcsec per pixels (as proposed in the SLOAN Digital Sky Survey) this would $\Rightarrow$ 160 Mbytes / deg$^2$ per passband, or many Tera-bytes of data for a "sky" survey. Digitised photographic sky surveys have been successfully processing equivalent volumes of data for many years making use a concept summarised in the "Kibblewhite Diagram", shown in figure 2.

The basic concepts here are:

- most of the pixels ($\sim$90%) in a survey frame belong to the smoothly varying sky background and hence can be accurately represented using **much** lower resolution sampling;
- images can be defined to be those regions of contiguous pixels lying above some user-specified threshold relative to local sky;
- most of these images are faint with little information content other than that reducible to simple descriptors such as position, intensity and shape parameters;
- all stellar images can in principle be parameterised with no loss of information using just position and intensity (although in practice the shape descriptors are necessary to judge which images are stellar);
- this leaves only a handful of bright galaxies where more detailed pixel mapping may be necessary to fully extract the information required.

This straightforward concept leads to an enormous data compression ($\times$100) with little

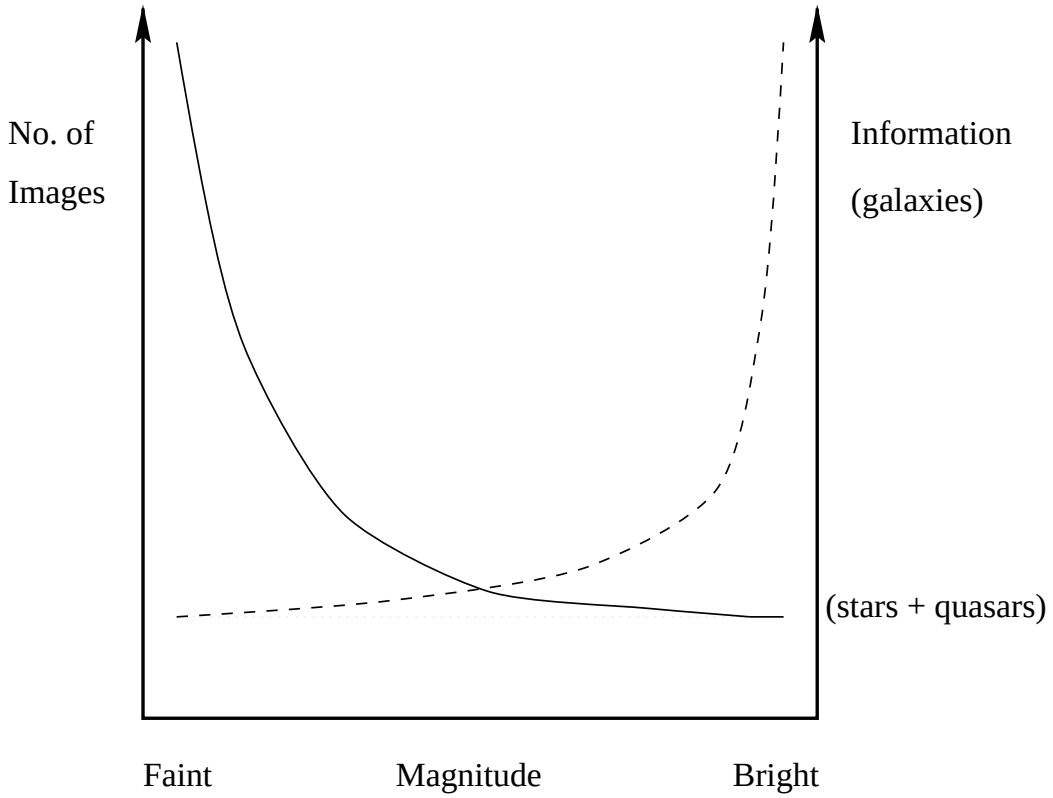


KIBBLEWHITE DIAGRAM

FIGURE 2. A Schmidt Sky Survey plate contains 4 Gbytes of data. Detecting and parameterising objects results in a large data compression $\sim \times 100$ with only a small loss of information.

---

or no loss of pertinent information. Furthermore by collecting only relevent detected image parameters, subsequent steps in the analysis become much easier.

Optical object catalogues covering large areas of sky have now been produced by several different groups (see Lasker, 1995b and references therein) and are generally available on-line at various INTERNET sites. Below is a brief summary of the main object catalogues now available and under construction.

Southern Hemisphere; UKST $B_J = 22.5$ and $R = 21.0$

- $B_J$ digitised at 2 arcsec resolution by COSMOS – catalogue
- $B_J$ and R will be digitised by SUPERCOSMOS – pixels + catalogue
- $B_J$ digitised at 3 arcsec resolution by STSCI – pixels + GSS
- R being digitised at 2 arcsec resolution by STSCI – pixels + new GSS
- $B_J$ and R to $|b| > 20$ deg at 1 arcsec resolution by APM – catalogue

Northern Hemisphere; POSS1 O = 22.0 and E = 20.5; Quick V = 19

- O and E digitised at 2 arcsec resolution by APS – catalogue
- V digitized at 3 arcsec resolution by STSCI – pixels + GSS
- O and E digitised to $|b| > 20$ deg at 1 arcsec resolution by APM – catalogue

Northern Hemisphere; POSSII $B_J = 22.5$, R = 21.0, I = 19.0

- being digitised by STSCI, APM, SUPERCOSMOS, APS .....

There are typically 1/4–1/2 million objects detected on each photographic survey plate and between 1500 and 2000 plates required to cover the whole sky in just one passband. These object catalogues contain magnitude, colour and shape information on around 1 billion objects and in conjunction with the compressed pixel maps compiled by STSCI have become the fundamental database for most of wide field survey astronomy.

### 1.4. *Next Generation Optical Surveys*

Until recently CCD arrays have been physically small and the pixel sizes not well matched to the plate scales available on potential wide field survey telescopes. In addition there has been the problem of what to do with the vast amounts of data that a CCD sky survey would produce. These drawbacks now no longer limit the potential for CCD-based sky surveys - large format 2048 × 2048 and 2048 × 4096 CCDs are now available and still larger mosaics ranging from 4096 × 4096 to 8192 × 8192 pixels are being fabricated, *e.g.* Luppino *et al.* (1994), Boronson *et al.* (1994); whilst computing resources and storage media have advanced sufficiently to enable both full archiving and "real-time" processing of a CCD-based survey to take place. Thinned CCD mosaic cameras will have efficiencies $\eta \sim 70\%$ and on a medium size telescope (2-3m) will typically cover a field of area $A \sim 0.25\mathrm{deg}^2$, leading to an effectiveness, $\eta \times A \sim 0.2$, approaching that of photographic surveys.

Although the existing photographic surveys cover the whole sky there is no requirement that a fainter CCD-based survey should do the same. Significant scientific progress will be made by: exploiting the large gains in efficiency, particularly in the U and I-bands; by going 10 times fainter and exploiting the factor of 5 or so higher accuracy; and from the better image quality – seeing ∼1 arcsec rather than the 2–3 arcsec of current survey material. In a recent review, Kron (1995) summarised the current and near–future CCD surveys that are being undertaken. Borrowing from this review and updating it as necessary, the following list indicates the current and near–future status of CCD mosiac cameras capable of doing survey work. The list is undoubtedly incomplete but hopefully provides an indication of the current state-of-the-art in this field. For more details on many of these systems consult Kron (1995) and the references therein.

- LACCD – Tyson and collaborators, Tyson *et al.* (1993); 2 × 2 array of thick Tek CCDs 2048 × 2048 with 24$\mu$ pixels; for use on Steward 2.3m, CTIO 4m, NOAO 4m; $\equiv 0.5 \times 0.5$ deg$^2$ on the 4m telescopes

- Kiso Mosaic Camera – Sekiguchi *et al.* (1992); 8×5 array thick TI CCDs 1000×1018 of 12$\mu$ pixels; used on Kiso Schmidt, Swope 1m Las Campanas $\equiv 0.7 \times 0.5$ deg$^2$, 4.2m WHT (March 96); $\equiv 0.6 \times 0.4$ deg$^2$

- MACHO project - Microlensing toward Galactic Bulge and LMC; Stubbs *et al.* (1994);

**two** $2 \times 2$ array thick Ford/Loral $2048 \times 2048$ of $15\mu$ pixels – simultaneous B and R filters; dedicated telescope Mt. Stromlo 1.3m; $\equiv 0.7 \times 0.7$ deg$^2$ twice !

• MOCAM - CFHT (1995); $2 \times 2$ array thick Loral $2048 \times 2048$ of $15\mu$; CFHT 3.6m common user instrument; $\equiv 0.3 \times 0.3$ deg$^2$

• NOAO - Boronson *et al.* (1994); $2 \times 2$ array thick Loral $2048 \times 2048$ of $15\mu$ pixels; next generation $8192 \times 8192$ array from 2k $\times$ 4k Loral CCDs; used on KPNO 0.9m, 4m; $\equiv 0.5 \times 0.5$ deg$^2$

• Univ. of Hawaii - Luppino *et al.* (1994); $4 \times 2$ array thick Loral $2048 \times 4096$ of $15\mu$ pixels; used on UH 2.2m; $\equiv 0.25 \times 0.25$ deg$^2$

• SDSS - Sloan Digital Sky Survey York *et al.* (1993); $6 \times 5$ array thin Tek $2048 \times 2048$ CCDs with $24\mu$ pixels – drift scan simultaneous U,G,V,R,I filters; to be based at Apache Point with dedicated 2.5m telescope; $\equiv 0.2 \times 1.4$ deg$^2$ times five passbands

• INT WFC - common user instrument see Irwin (1992); $2 \times 2$ array of thinned Loral $2048 \times 2048$ CCDs with $15\mu$ pixels; to be used on 2.5m INT; $\equiv 0.4 \times 0.4$ deg$^2$

Although at present there are no actively operating thinned CCD mosaic cameras, many of the systems in the preceding list are planned to be upgraded to thinned systems as and when such devices become readily available.

### 1.5. *Surveys in other Wavebands*

The last decade has seen a renaissance of wide field surveys in other wavebands. Coupled with the optical catalogues these surveys provide one of the main sources of objects for both deep single object slit spectroscopy on 4+m class telescopes and for the wider area multi-object spectrographs such as WYFFOS, 2DF, HYDRA ... Indeed many objects currently being studied in great detail on the Keck telescope were originally discovered using the wide field surveys resource.

The following list gives a necessarily brief summary of some of the major non–optical wide area surveys already completed or on the near horizon.

• X-ray surveys – all sky catalogues include Uhuru (1970-73); HEAO-1 (1977-79); Ariel V (1974-1980); Einstein/EMSS (1978-81); ROSAT WFC with ≈50,000 sources; in the pointed mode the ROSAT HRC has been used to survey >1000 deg$^2$ of sky; current and future missions include ASTRO-D, AXAF and XMM; see Bradt *et al.* (1992) for a comprehensive review of X-ray missions.

• Infra-red surveys – notable here are the IRAS all sky survey at 12,25,60,100$\mu$ to flux limits of 0.2–1Jy, with ≈250,000 sources catalogued; and the recently launched ISO mission which will survey a limited region of sky but with better resolution and to much fainter flux limits than possible with IRAS.

• Near IR surveys – two major surveys are currently in progress; DENIS plans to map the southern sky in I,J,K with 1–3 arcsec sampling to a limit of $m_k$ ∼14–15 using a dedicated 1m telescope; while 2MASS is an all sky survey at 2.5 arcsec sampling in J,H,K using a 1.3m telescope; both of these surveys will produce catalogues of several million sources with coordinates accurate to ∼1 arcsec; the review by Price (1988) covers IRAS and earlier Near IR surveys.

• Radio surveys – there are many large sky coverage radio surveys already completed or nearing completeion with flux limits ranging from ≈ 0.1 – 1Jy including Cambridge 2c – 8c and variants within; Parkes–MIT–NRAO; Greenbank87; MG and so on...; major

new surveys are the NVSS 20cm survey to a flux limit of 2.5mJy over 30,000 deg$^2$ of sky; and FIRST, a 10,000 deg$^2$ survey to a flux limit of 0.7mJy; combined, these surveys will produce catalogues of several million sources with coordinates accurate to $sim1$ arcsec; see for example Becker, White & Helfand, (1995).

### 1.6. *The Likelihood of an Identification*

A major requirement for all these non–optical surveys is the ability to rapidly access and identify the counterpart objects from optical sky catalogues, with minimal contamination from spurious mis-matches. In particular, when searching for intrinsically rare objects the mis-matching rate often beomes the limiting factor in the success or otherwise of the scheme. An example of this would be in looking for, say, IR detected objects that have no apparent optical counterpart to some optical flux limit. If the combined (optical + IR) positional error box is small the probabilty of getting an accidental match is correspondingly low. We can quantify this problem by considering the likelihood of identification.

Following Prestage & Peacock (1983) and assuming radially symmetric Gaussian errors for simplicity (generalisation is relatively straightforward); the probability of detecting an object at a distance r from the expected position is by the Rayleigh distribution

$$P(r \rightarrow \delta r|id) = \frac{r}{\sigma^2} exp(-\frac{r^2}{2\sigma^2}).\delta r \tag{1.2}$$

where $\sigma^2$ is the combined variance in position expected. The probability of finding a confusing source at this distance is simply

$$P(r \rightarrow \delta r|c) = 2\pi r\rho.\delta r \tag{1.3}$$

where $\rho$ is the average cumulative surface density of sources up to some chosen limiting magnitude. This surface density could be further subdivided on say morphology (eg. stellar, non-stellar), colour and so on. Now from Bayes' theorem we know that

$$P(id|r) = \frac{P(id).P(r|id)}{P(id).P(r|id) + P(c).P(r|c)} \tag{1.4}$$

$$P(c|r) = \frac{P(c).P(r|c)}{P(id).P(r|id) + P(c).P(r|c)} \tag{1.5}$$

where $P(id|r)$ is the probability that the object at $r$ is the correct identification; $P(c|r)$ is the probability of it being a confusing object; and $P(id)$ and $P(c)$ are respectively the prior probabilities that the identification is visible at the chosen limiting magnitude and that confusing objects are visible. Clearly, in general optical identification work, $P(c) = 1$ since confusing objects are both visible and greatly outnumber correct identifications. In the case of relatively bright identifications $P(id) = 1$ since it is the probability that the proposed source is reliable. For faint identifications $P(id) < 1$ since it is the combined probability of the proposed counterpart being reliable, coupled with the probability of the source being optically visible to this magnitude limit.

Therefore by rearranging the preceding equations we have that

$$P(id|r) = \frac{P(id).L(r)}{P(id).L(r) + 1} \tag{1.6}$$

and that

$$P(c|r) = \frac{1}{P(id).L(r) + 1} \tag{1.7}$$

where the likelihood ratio $L(r)$ is defined by

$$L(r) = \frac{P(r|id)}{P(r|c)} = \frac{exp(-r^2/2\sigma^2)}{\sigma^2.2\pi\rho} \tag{1.8}$$

It is straightforward to see that the smaller the combined error search radius $\sigma$ the easier it becomes to deal with confusing sources. In particular as non-optical surveys reach ever fainter flux limits the confusion problem becomes significantly worse, without a concomittant improvement in positional errors; since $P(id)$, the probability of the optical identification being visible, will also decrease.

## 2. Optical Telescope Design Constraints on Wide Field Imaging

Although almost all telescope design is now done using ray-tracing packages there are several aspects of optical telescope design amenable to simple analytic analysis. In quite general terms this aproach can be used to highlight the problems of using large telescopes for wide field survey work and in particular provides a useful approximate starting point for evaluating proposed wide field imaging designs.

### 2.1. *Aperture, Scale and Depth of Focus*

Definitions: Effective focal length (m) - $F$; aperture/diameter (m) - $D$; focal ratio - $f = F/D$; semi-aperture angle - $u'$. Units as in () unless otherwise stated.

In most optical work the diameter of the entrance pupil, $D$, of the telescope is sufficiently large that the angular size of a diffraction limited image, $\xi$, of a point source given by

$$\xi = 1.2\frac{\lambda}{D} = 0.14 \times (\frac{\lambda}{5500\mathring{A}}) \times (\frac{1m}{D}) \quad arcsec \tag{2.9}$$

is significantly smaller than imperfections caused by the telescope optics or the point spread function (psf) due to atmospheric or dome seeing. The latter two effects are usually the dominant contributors to the psf.

First-order approximation (Gaussian theory) to the optical performance of a telescope assumes that apertures and field size are small compared to the focal length. With this approximation, $\theta$, the inclination of any ray to the optical axis satisfies $sin(\theta) \approx \theta$ and $cos(\theta) \approx 1$, and we can see immediately from figure 3 that the angular scale in arcsec/mm, is given by

$$scale = \frac{d\theta}{dx} \simeq \frac{206}{Df} \tag{2.10}$$

Therefore, two objects separated by an angle $\theta$ on the sky will appear a distance $= \theta/scale$ apart at the focal plane of the telescope. For an 8m telescope with an f/16 secondary, such as Gemini, this implies a focal scale of 1.6 arcsec/mm. Even on an 8m telescope designed for prime focus imaging, such as the f/2 prime on SUBARU, the image scale is a daunting 12.9 arcsec/mm – the proposed 30 arcmin field of view will require a detector of order 140mm × 140mm in size.

Using a similar construction, illustrated in figure 4, we can derive the depth-of-focus, $\delta z$, over the focal plane,

$$Depth - of - focus = \delta z \approx \frac{\text{FWHM}}{\text{Scale}} \times f \tag{2.11}$$

where FWHM is the Full Width at Half Maximum of the seeing profile.

For a telescope giving good imagery the sine condition is satisified so that the Numerical

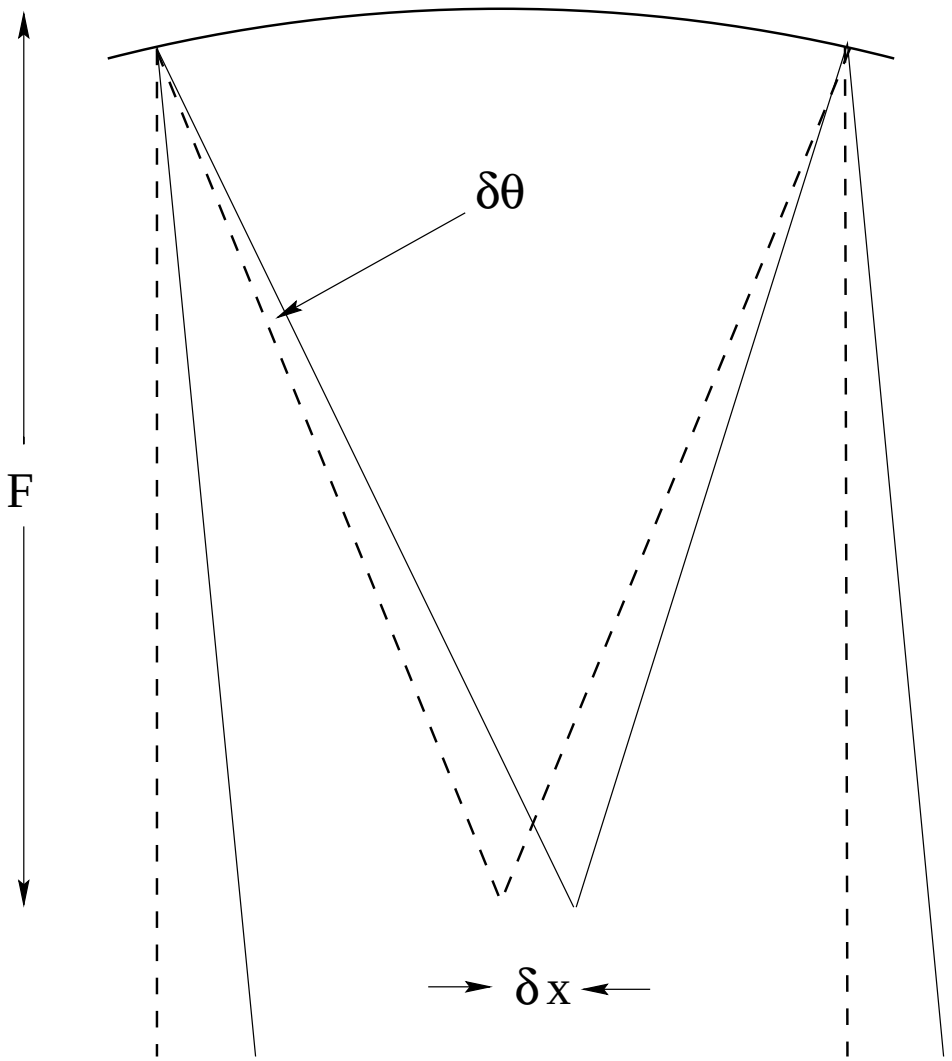


FIGURE 3. Equivalent system for deriving image scale. A change in entrance angle $\delta\theta$ gives an image shift $\delta x = F \times \delta\theta$.

---

Aperture $sin\ u' = 1/2f$. If in such a system we chose to match the pixel size, $p$ (microns) to the expected best seeing FWHM (arcsec), to efficiently sample the sky, then

$$F \approx \frac{2p}{\mathrm{FWHM}} \times 0.206 \tag{2.12}$$

and therefore

$$sin\ u' \approx \frac{D \times \mathrm{FWHM}}{4p} \times 4.85 \tag{2.13}$$

As an example consider a pixel size, $p = 15\mu$; and a telescope situated on a good site where the average best seeing had a FWHM = 0.5 arcsec;

- 4-m telescope $sin\ u' \approx 0.16(f/3.1)$ – several 4m-class systems exist
- 8-m telescope $sin\ u' \approx 0.32(f/1.5)$ – corrected field difficult

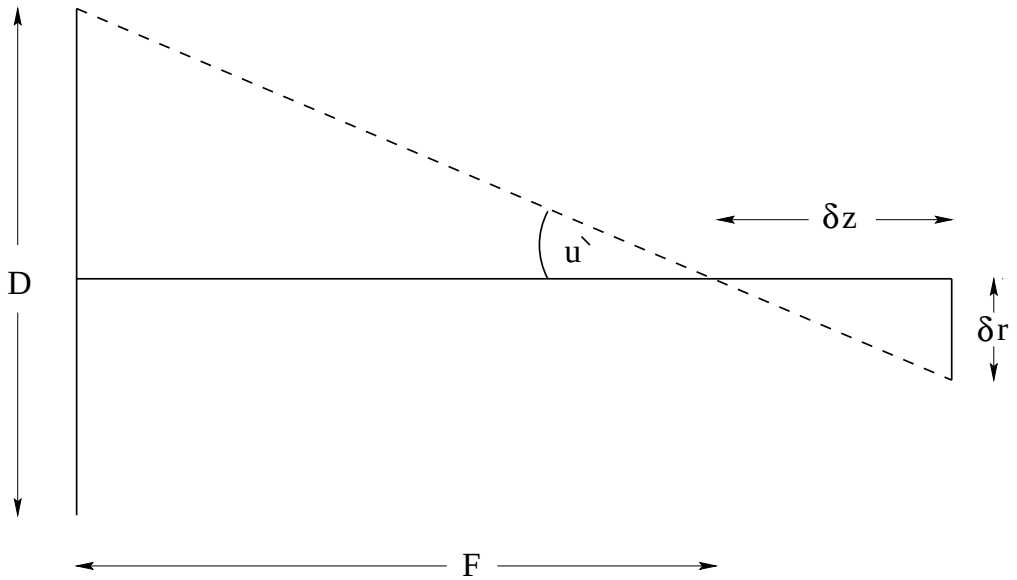


FIGURE 4. Depth of focus $\delta z$ to give image spread $\delta r$. For good imagery $sin\ u' = 1/2f$ and $\delta r = \delta z \times tan\ u' \simeq \delta z/2f$.

---

- 16-m telescope$sin\ u' \approx 0.64(f/0.8)$ – impossible?

The field of view depends on the off-axis vignetting, including the effects of sky baffles, and the optical aberrations inherent in the particular telescope design. The latter limitation can usually only be adequately investigated using detailed ray tracing. However, with the current limited size of CCD detector arrays (≈120mm × 120mm for a state-of-the-art 8192 × 8192 mosaic), it is often the detector that limits the useful field of view.

### 2.2. *Cassegrain Telescopes*

Seidel's (1856) 3rd order theory predicts the amounts of: spherical aberration, coma, astigmatism, field curvature and distortion. For example, at prime, a single paraboloidal mirror with no correcting elements will provide seeing-limited images on axis. Any other form of mirror, spherical, ellipsoidal or hyperboloidal gives fuzzy images, affected by spherical aberration. To give good image quality over a wide field of view requires the use of a prime focus corrector – generally a refractive multi-element system of low optical power. The diameter of the correcting elements is limited by glass manufacturing technology to around a maximum of 1 meter. In turn this is usually the limiting factor in the maximum possible physical size of the prime focus field, which because of the fast focal ratio (∼2) and vignetting limitations, leads to a typical maximum field of order 1/2 meter diameter.

An alternative approach is to use a two mirror system and place the instrumentation at the secondary focus. In a classical Cassegrain system the primary mirror is a concave paraboloid and the secondary a convex hyperboloid. Typcal secondary Cassegrain focal ratios are f/6 to f/20 and the field of view is generally modest (∼10 – 20 arcmins). The field of view is limited by several factors including: aberrations, the hole in the primary, sky baffles, size of correctors at prime and so on. A schematic drawing of a classical Cassegrain telescope showing the different focii is shown in figure 5. The secondary

image is usually formed a moderate distance behind the primary mirror, which needs to be perforated. The relationships between the focal lengths, radii of curvature of the mirrors, their separation and placement with the respect to the primary are all determined by simple geometrical optics.

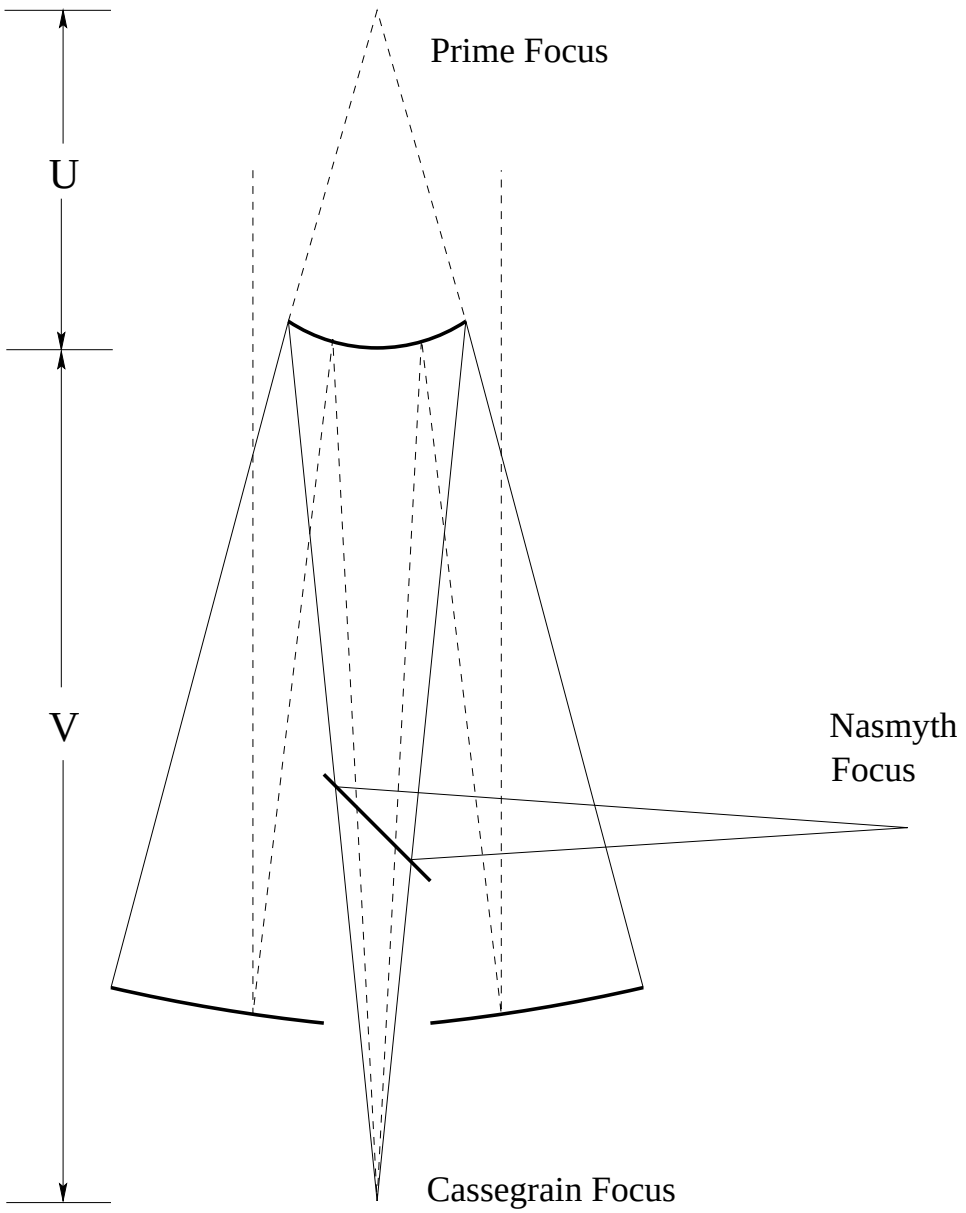


FIGURE 5. Schematic of a Cassegrain Telescope showing the different focii. The main text indicates how the primary mirror diameter, $D_1$, and f/ratio, $f_1$, and secondary mirror effective diameter, $D_2$, and f/ratio, $f_2$, are interlinked with the placement of the secondary, $U$, and the position of the final Cassegrain focus, $V$.

The focal length of the secondary, $F_2$, is given by

$$\frac{1}{F_2} = \frac{1}{V} - \frac{1}{U} \tag{2.14}$$

where $U$ is the distance of the secondary inside the primary focus (see figure 5), forming a secondary image at a distance $V$. Usually

$$U + V = F_1 + (0.5 \sim 1.0)D_1 \tag{2.15}$$

in order to place the secondary focus at a convenient location, and we also have from direct trigonometric construction

$$U = F1 \times \frac{D_2}{D_1} = f_1 \times D_2 \tag{2.16}$$

where $D_1$ is the diameter of the primary, $D_2$ the effective diameter of the secondary; and

$$V = f_2 \times D_2 \Rightarrow f_2 = \frac{V}{U} \times f_1 \tag{2.17}$$

(The real diameter of the secondary would be some $\sim$10% larger than the effective diameter to ensure no vignetting of a finite field.) One final link in the chain is to note that in the absence of astigmatism the curvature of the Petzval surface coincides with the curvature of the final focal surface, see for example Willstrop (1985). The curvature of the Petzval surface of a system of mirrors, $R_p$, is related to the the radii of curvature of the mirrors, $R_i$, by

$$\frac{1}{R_p} = \sum_{i=1}^{n} \frac{2}{R_i} = \sum_{i=1}^{n} \frac{1}{F_i} \tag{2.18}$$

where $F_i$ is the focal length of mirror $i$ and the convention is to take the + sign for convex surfaces and $-$ sign for concave surfaces. The linear magnification, $m$, produced by the secondary is $V/U$ and if the secondary image is to be free of spherical aberration then its eccentricity, $e_2 = (m+1)/(m-1)$. Images at the secondary focus are still affected by coma and astigmatism and of course field curvature. The angular image spread due to coma, $\delta\theta$, at radius $\theta$ is given by

$$\frac{\Delta\theta}{\theta} = \frac{3}{16 \times f^2} \tag{2.19}$$

which also holds for uncorrected prime focus images. Due to the typically long Cassegrain focal lengths, f/10 – f/20, the comatic blur only reaches 1 arcsec at around 1/2 degree radius, which is normally considerably larger than the field of view used.

As an example consider the WHT: it has a primary $f_1/2.5$, $D_1 = 4.2$m, $\Rightarrow F_1 = 10.4$m; and a secondary $f_2/11$. Equations 2.15 – 2.17 imply that

$$U + V = D_2 \times (f_1 + f_2) \Rightarrow D_2 \approx 1 \tag{2.20}$$

and therefore in conjunction with equation 2.14 this tells us that

$$D_2 = 1 \Rightarrow F_2 = -3.1; U = 2.5; V = 11.0 \tag{2.21}$$

and the radius of curvature of the Cassegrain focal surface is 4.4m. It is straightforward to estimate if this radius of curvature is a problem by considering the change of planar depth, $\delta z$, of the surface as a function of angular distance, $\theta$, from the optical axis

$$\delta z \simeq R_p \times \frac{\theta^2}{2} = \frac{r^2}{2R_p} \tag{2.22}$$

where $r$ is the radial distance from the optical axis. If $R_p = 4.4$m, at a radial distance of $r = 5$cm, $\delta z = 280\mu$; cf. to the depth-of-focus $\approx 1200\mu$, ie. no problem.

### 2.3. *Ritchey–Chrétien Telescopes*

Ritchey–Chrétien telescopes are two-mirror Cassegrain-like telescopes with a realtively large secondary field of view. In this case both the primary and the secondary mirrors are hyperboloids and the secondary focus is completely corrected for spherical aberration and coma. Prime focus imaging without correcting elements is ruled out, however, it turns out that it is easier to design a wide field corrector for a hyperboloidal mirror than for a paraboloidal Cassegrain system. In practice, Ritchey–Chrétian telscopes offer some of the biggest fields available on large telescopes, both at prime and at Cassegrain. For example, the 3.9m AAT has a 40 arcmin field at Cassegrain and a new 4-element prime focus corrector gives a 2 degree field at prime.

The Gemini 8m telescopes will follow a Ritchey-Chrétian design with an $f_1/1.6$ primary. An $f_2/6$ wide field secondary option was originally considered, but note that equations 2.14–2.17 $\Rightarrow D_2 \approx 2.5$m, a huge secondary mirror; whereas the adopted $f_2/16$ secondary, which all that is currently funded, $\Rightarrow D_2 \approx 1$m. In the latter case, equation 2.18 implies that the radius of curvature of the secondary focus will be around 1.8m without further correcting optics.

Another interesting design is provided by the 2.5m telescope under construction for the SLOAN Digital Sky Survey. This uses a secondary mirror of equal (and opposite sign) radius of curvature to the f/2.2 primary to give a flat focal plane secondary f/5 field. The relatively fast f/5 secondary is needed to provide matched sampling at the image detector plane; whilst the flat focal plane greatly simplifies both direct imaging instrumentation and the multi-fibre spectrograph design. With $F_2$ fixed and equal to $-F_1$, $U$ and $V$ are completely determined from the preceding equations, which in turn fixes the diameter of the secondary mirror to be $\sim$1.3m and leads to a field of view of order 30 arcmin. This telescope will be used for imaging with CCDs in the drift scan mode and therefore has two aspheric plate refractive correcting elements, situated near the focus, to eliminate field distortion.

Although the SLOAN solution to the wide field imaging problem works well for telescopes of relatively modest aperture, the flat field constraint coupled with the relatively fast secondary focus, necessary to give a good image scale, leads to large diameter secondary mirrors, and would be impractical for 8m-class telescopes.

### 2.4. *Field Distortion*

Uncorrected field distortion at either primary or secondary focii in Cassegrain-type systems take the form of

$$\theta_{true} = \theta \times (1 + k1 \times \theta^2 + k2 \times \theta^4 + ...) \tag{2.23}$$

As an example, at WHT prime:

$$k1 \times \theta^2 = -0.000027 \times (\frac{\theta}{\mathrm{arcmin}})^2 \tag{2.24}$$

whilst at WHT Cassegrain the field distortion is negligible.

Field distortion can also be important in the so-called point and stare mode of operation. It is now common practice to stack sequences of offset CCD frames to reach deeper limiting magnitudes. In shifting the frames to coalign them before coaddition, it is necessary at the same time to allow for the effects of differential field distortion across the frame. For WHT prime, at a radius of 10 arcmin, the differential field distortion relative to the optical axis is over 1.5 arcsec.

### 2.5. *Alternative Wide Field Telescopes*

The commonest form of wide field survey telescope is the Schmidt camera. Schmidt telescopes have a spherical primary with a radius of curvature equal to the length of the telescope tube. An aspheric corrector plate placed at the entrance aperture corrects for spherical aberration and also defines the limiting diameter of the telescope. The primary advantage of a Schmidt telescope is the enormous field of view. For example the UK Schmidt telescope (UKST) has a 6 degree field which it obtains with a 1.2m aperture and a 1.8m mirror. Disadvantages are that the focal plane is curved and located internal to the telescope tube; the tube length is large for a given diameter and practical f/ratio; but the major disadvantage is that simply scaling up the design to significantly larger apertures is impractical because of the problems of both making and supporting large refractive elements.

There have been many alternative wide field designs proposed, of which one of the most promising for large aperture work is based on a three mirror system. Willstrop (1985) describes a flat-field Mersenne-Schmidt telescope which covers a field 3 degrees in diameter with images smaller than 0.5 arcsec in extreme spread; over the central 2 degrees the images are smaller than 0.1 arcsec. For more details consult the article by Willstrop (1985). More recent work by Willstrop (private communication) has pushed this design further and lead to a practical design for a 5m diameter telescope having a 5 degree field of view with images better than 0.5 arcsec over the entire field.

## 3. Wide Field Detectors

The traditional detector for wide field imaging over the last century has been the photographic plate. Modern IIIaJ, IIIaF, IVN (plates) and 4415 emulsions (film) provide very large area detectors, $\approx$40cm $\times$ 40cm in size, that are cheap, astrometrically stable to the level of microns and relatively simple to use. The active element, silver halide grains, are a few microns in size, and give a detective quantum efficiency between 1–5%. Although this figure is relatively poor by modern standards, as outlined in section 1., it is the product of this efficiency and the area covered, that really matters.

Historically, the earliest successful and most widely used large area electronic detectors, were the image intensifier systems of which the IPCS (Bokensburg, 1972) is probably the best known. IPCS systems were the instrument of choice for faint spectroscopic work throughout most of the last decade. However, gradually over the last twenty or so years, Charge Coupled Devices (CCDs) have become the preferred detector for most applications. Since there are many excellent review articles on CCD development (eg. Janesick & Elliot, 1992) there is no point in repeating the story here. Over the last decade the active area of CCDs has grown dramatically from the typical $22\mu$ pixels of $576 \times 384$ CCDs available in the late 1980's, through the current generation of $24\mu$ pixel $2048 \times 2048$ thinned Tektronix CCD workhorse devices, and on to the new generation of thinned CCD mosaics of typically $15\mu$ pixels and total array sizes of $4096 \times 4096$, or even, $8192 \times 8192$ pixels.

As we are interested in potential wide field detectors, for both imaging and spectroscopic applications, I have summarised the relative merits and disadvantages of the most commonly used wide field detectors in table 1 and indicated a few references for further reading.

High resolution spectroscopy, and usually only in the range 3200Å– 4000Å, is the only remaining area where an IPCS-type detector offers potential advantages over a thinned blue sensitive CCD. We can see why this might be the case by considering the

| Detector | Advantages | Disadvantages |
|---|---|---|
| Photography<br>Plate IIIaJ,IIIaF & IVN<br>Films 4415[1] | Wide area astrometry<br>Very large area<br>(≈40cm × 40cm)<br>Inexpensive<br>Simple to implement<br>Eyeball inspection | Low efficiency<br>Grain noise high<br>Non-linear<br>Small dynamic range<br>Not reproducible<br>Needs digitising |
| Image Photon Counting<br>Systems – IPCS<br>MIC, BIGMIC[2] | Good blue QE ∼25%<br>Up to 70mm diameter<br>Monitor in real time<br>Zero readout noise<br>Selectable pixel size<br>No cooling required | Poor red QE <5%<br>Fragile – overexposure<br>Only low photon rates<br>Field distortion |
| CCDs | Excellent QE blue – red<br>(QE ∼70%)<br>Temporal stability<br>Large dynamic range<br>Linear response<br>Low readout noise<br>Insensitive to overexposure<br>No photon rate constraints | Still limited area<br>No real time image<br>Inflexible pixel sizes<br>Cooling required |

[1] See articles by Hartley (1994) and Parker *et al.* , 1994 for details of photographic emulsions.
[2] See article by Fordham *et al.* (1994) for more details of modern IPCS systems.

TABLE 1. Wide Field Detectors

signal:to:noise produced by the two types of detector. In a general sense, the observed counts per detector pixel,$x_i$, for an exposure of length t, are determined by three factors

$$x_i = s_i \times t + b_i \times t + r \tag{3.25}$$

$s_i$ – the signal photon rate in pixel $i$; $b_i$ – the background photon rate; $r$ – the readout noise per pixel. Assuming unit gain, ie. 1 $e^-/\gamma$ per ADU, and ignoring spurious noise sources for simplicity, the potential signal:to:noise, $S:N_i$, for a Poisson process for pixel $i$ is given by

$$S:N_i = \frac{s_i \times t}{\sqrt{(s_i + b_i)t + r^2}} \tag{3.26}$$

which translates to two limiting cases: detector noise limited where

$$S:N_i \simeq \frac{s_i \times t}{r}; \quad r^2 > (s_i + b_i)t \tag{3.27}$$

and photon noise limited where

$$S : N_i \simeq \frac{s_i}{\sqrt{s_i + b_i}} \times \sqrt{t}; \quad r^2 < (s_i + b_i)t \tag{3.28}$$

Since an IPCS based system produces zero readout noise it always operates in the second, photon noise limited regime. Gilmore & Walton (1993) illustrated the advantages of the IPSC-2 photon counting system and a thinned Tek CCD using the Utrecht Echelle Spectrograph on the WHT. With the maximum practical CCD exposures limited to around 1 hour (because of cosmic rays) the total signal per pixel was <10 counts and the CCD readout noise (5 $e^-$), rather than the photon noise dominates. However, the advantage is finely balanced and if the same experiment were carried out on a 10m telescope, the better blue efficiency of the best thinned CCDs, coupled with the higher photon rate at the detector, would switch the advantage back to the CCD. Figure 6 shows an example of the spectral response curves for the CCDs currently available at the Isaac Newton Group of telescopes on La Palma. With suitable treatment, eg. thinning and coating, it is feasible to have CCD QEs >50% over most of the optical passbands.

### 3.1. *A Basic Description of CCDs*

A CCD (Charge Coupled Device) is a multi-layered sandwich of various silicon- based wafers ($\sim \mu$'s deep) supported on a relatively thick ($\sim 100\mu$) silicon substrate. The basic structure is illustrated in figure 7. The conducting electrodes on the surface are insulated from the p-type silicon substrate by a thin layer of $SiO_2$. These electrodes are made from "light–transparent" polysilicon (polycrystalline silicon). Column isolators are used to define the CCD columns as buried channels, while the polysilicon electrodes define the rows. Each pixel is formed by 3 adjacent surface electrodes plus the buried channel column isolators. The central electrodes of each trio are held at a positive voltage, the outer two at earth potential, and form a potential well near the front surface of the silicon substrate. This expells the majority carriers (holes) and produces a depletion layer. Incoming photons pass through the front layer of polysilicon electrodes and are absorbed by the silcon to produce hole-electron pairs in numbers proportional to the number of incident photons. These photo-generated electrons migrate to the depletion layer formed by the potential well and collect there as single charge packets, while their counterpart holes diffuse deeper into the underlying substrate. The array of "horizontal" electrodes (rows) above "vertical" charge-transfer channels (columns) defined by the column isolators, is known as buried-channel architecture. This desgin permits rapid and much more efficient charge transfer (CTE ~0.99999) compared with surface channel CCDs (see Janesick & Elliot, 1992 for more details).

The CCD can be thought of as a photosensitive array which generates electrons that are subsequently captured and stored as small buckets of charge. At readout time the pixels form a bucket brigade; each row of charge is passed down the columns and horizontally along the final row to be measured in turn and recorded digitially. This is accomplished by parallel sequencing the triads of electrodes with clocking waveforms of the type shown in figure 8. As each row reaches the bottom of the array it enters the horizontal register where a similar triplet of electrodes and clocking waveforms moves the packets across the register. On reaching the end-of-the-line, each charge packet is detected as a voltage across a capacitance, amplified by an on-chip amplifier, and digitised for subsequent output and storage. The next row is driven down and the sequence repeated until the CCD is cleared of charge. Typical "slow" readout times for a science grade CCD are of order 10–50$\mu$s per pixel, or $\approx$ 40– 200s for a 2048 $\times$ 2048 device.

The silicon band-gap between the valence and conduction bands is 1.14eV, which cor-

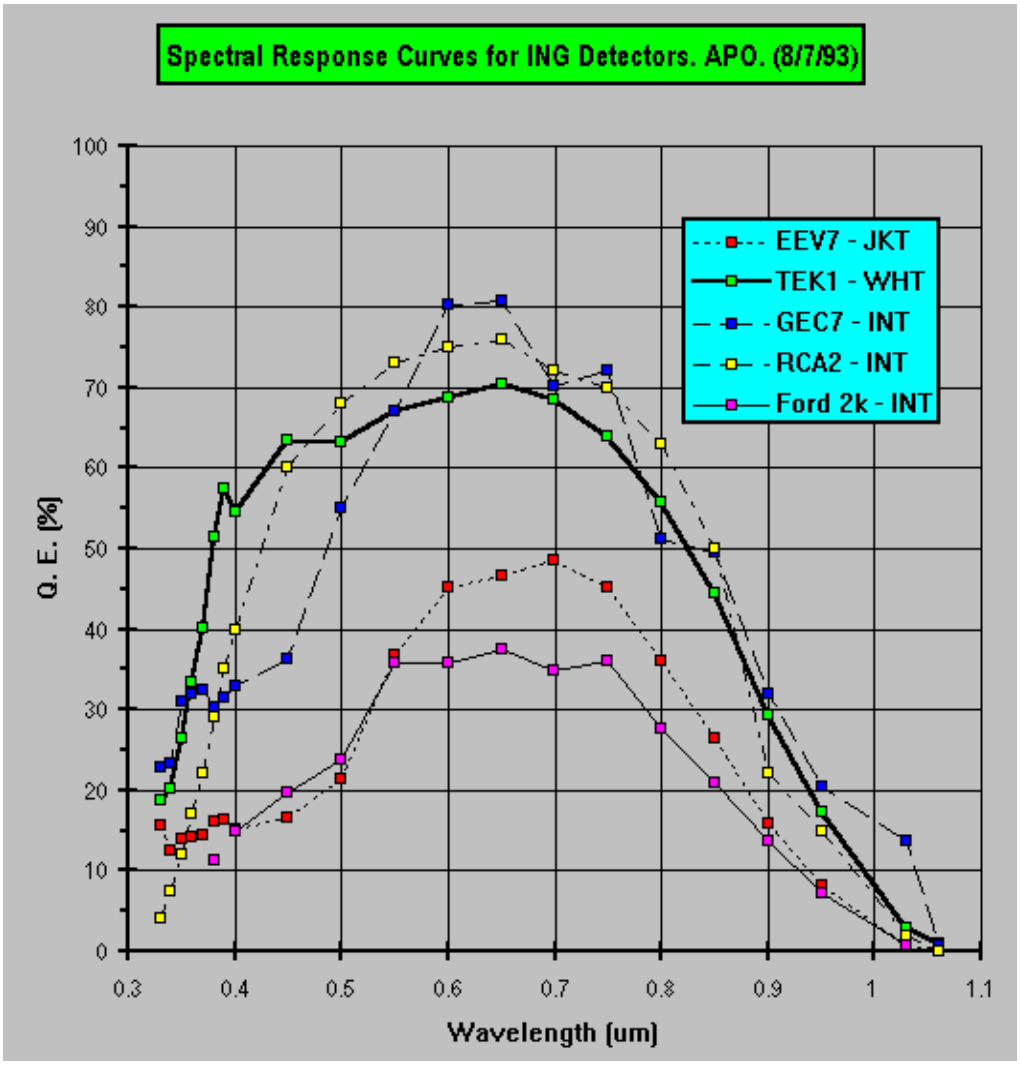


FIGURE 6. Spectral response curves for ING detectors. EEV7 is a thick blue–coated CCD; TEK1 is a standard thinned $1024 \times 1024$ device; GEC7 is a thinned equivalent of EEV7; RCA2 is an "ancient" thinned CCD; Ford 2k is a $2048 \times 2048$ Loral thick blue coated CCD. These devices are representative of the range of CCDs available on most telescopes. (Figure courtesy of Paddy Oates, Royal Greenwich Observatory)

responds to a wavelength of 10800Å. Between 1.14eV and about 5eV, each incoming photon will be potentially converted to $1e^-$ with a probability depending on the absorption depth, which varies from $0.2\mu$ at 2500Å to $500\mu$ at 10000Å. At still higher energies, CCDs are good X-ray detectors, the quantum yield is 1 $e^-$ / 3.65 eV. The exceptional efficiency at optical wavelengths of typical CCDs is illustrated in figure 6. There are several factors that contribute to limiting the CCD efficiency. In the case of a front-illuminated (thick) CCD (figure 7), the loss of efficiency in the blue is due to absorption of blue photons by the polysilicon electrodes; whilst at near IR wavelengths ($\sim$10000Å) the capture cross-section is the limiting factor. There is a also a general loss of photons due to surface reflection losses. At longer wavelengths the penetration depth can

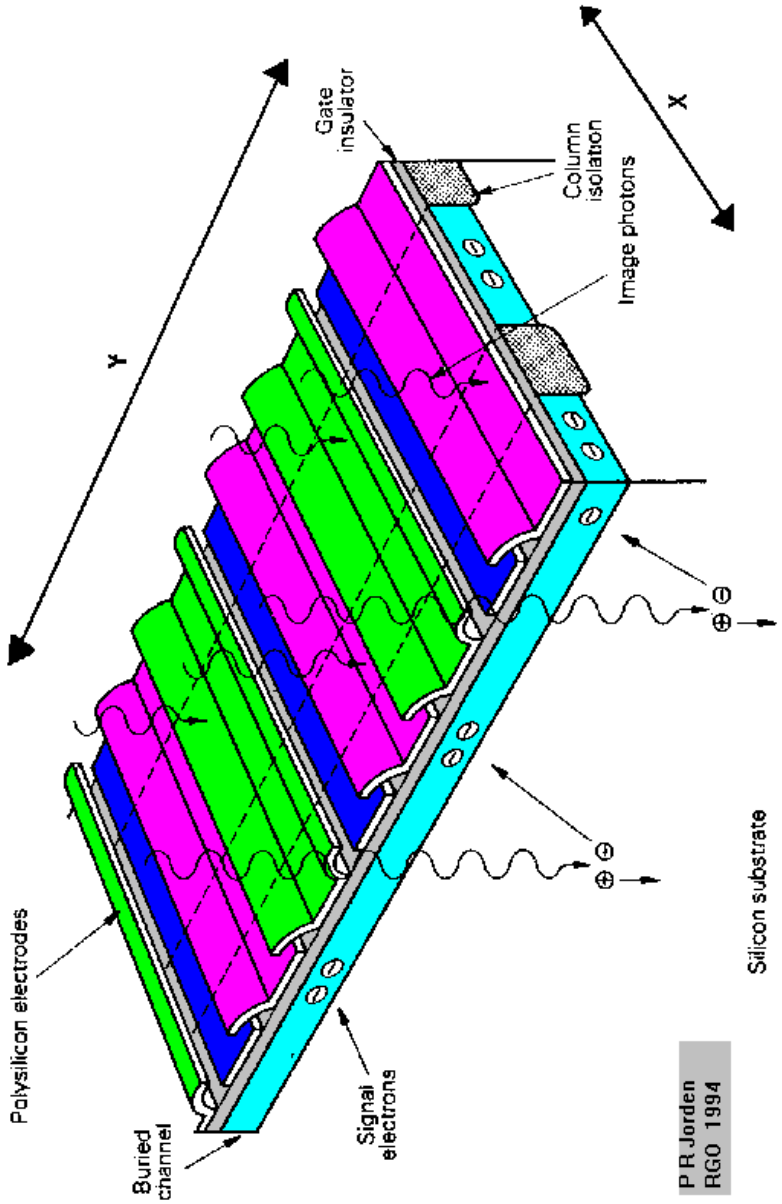


FIGURE 7. A schematic section of a CCD image sensor. (Diagram courtesy of Paul Jorden, Royal Greenwich Observatory)

be so large that losses due to recombination of hole- electron pairs becomes significant ($\tau_{recomb} \sim 100\mu$s). To improve the blue response of thick CCds a fluorescent coating can be applied to the front surface. This works by absorbing blue photons incident on the surface and re-radiating them at redder wavelengths. The redder photons pass more easily through the polysilicon electrodes. However, the blue response shortward of 4500Å is only improved from typically ∼5% to ∼15% by this process.

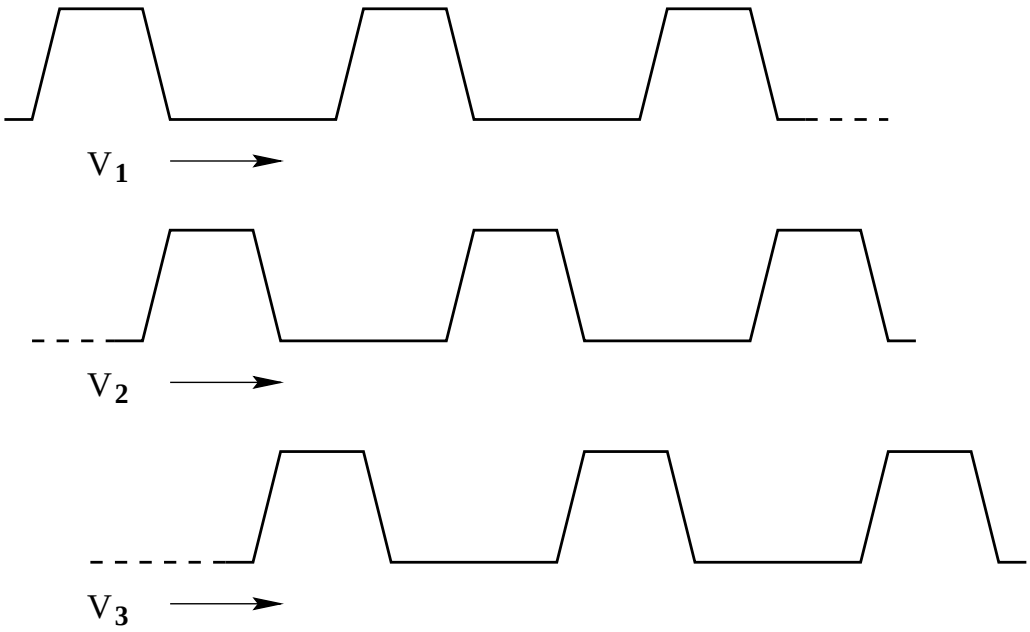


FIGURE 8. The Clocking Waveform used to Readout a CCD.

Thinned CCDs, formed by either acid etching or chemical/mechanical thinning of the backside silicon, employ silicon chips that are only $10-30\mu$ thick and can therefore be illuminated from the backside. This is still an art form as can be seen from the reviews given by Lesser (1989) and Lesser (1994), and the scarcity of large format thinned devices in operation. The thinning introduces several other problems such as: oxidation of the back surface which thereby aquires a net +ve charge drawing photo-generated $e^-$'s away from the depletion region – the effect is reduced by passivating the back surface or by UV flooding in $O_2$; the back surface is an excellent mirror and needs wavelength-tuned anti-reflection coating; thinned devices need some sort of mechanical surport such as bonding the front surface to a chip carrier; the thinned devices suffer from increasing fringing in the red due to internal reflection from front and back surfaces – not a problem in the blue due to the short optical path. The end result is that thinning dramatically improves the blue response, QE's of $\gtrsim$50% shortward of 4500Å are typical, by removing the obstacle of the electrode structure (figure 6). At the same time it might be thought that the long wavelength response, say toward 10000Å– near the silicon band-gap, should suffer because of the much reduced optical absorption depth. However, the problem/effect of multiple internal reflection of long wavelengths, that leads to fringing, also helps to compensate for the loss of silicon and in practice little degradation of red QE occurs.

A surprising feature of CCDs, given that the active depletion depth of $5–10\mu$ is a significant fraction of the pixel size, is the preservation of resolution with wavelength. There is some slight degradation of resolution due to spreading of photoelectrons before collection and some resolution loss due to imperfect charge transfer efficiency (CTE). The former effect is very difficult to detect in normal astronomical applications; while the latter manifests itself as low level smearing downstream from bright pixels. However, the internal structure of the CCD, particularly the electrode arrays and buried channels, do give rise to periodic intra-pixel variations in sensitivity (Jorden, Deltorn & Oates, 1994). These modulations are wavelength dependent and can cause problems in some situations

if the data is spatially undersampled. The spatial modulation in total recorded signal is worse for front-illuminated thick devices and amounts to some $\pm 10\%$ across columns, approximately independent of wavelength. As expected across rows (due to the electrode structure) the situation is worse with modulations of $\pm 25\%$ at 5000Å dropping to $\pm 10\%$ at 8000Å. For backside-illuminated thinned devices the spatial modulation at 5000Å is of order $\pm 1\%$ in both directions increasing to of order $\pm 5\%$ at 8000Å.

### 3.2. *Detector Requirements, Problems and Features*

Although this section is geared toward CCDs as the currently preferred detector of choice for wide field optical work, many of the requirements listed below are necessary for any potential wide field detector. For a detailed discussion about the problems caused by CCD "noise" sources and procedures to recognise and deal with them see the article by Gilliland (1992).

- Format – 2048 × 2048 pixels minimum; pixel size $8\mu$ to $30\mu$; the maximum physical size of an individual CCD is limited by the size and purity of currently available silicon wafers to an area of $\approx$ 20cm$^2$. The yield of larger science-grade devices is very poor. Larger areas are covered by using 3-edge buttable mosaic arrays with building blocks 2048 × 4096 CCDs, eg. Luppino *et al.* (1994).

- Readout noise – 4 to 6 e$^-$ routinely; best <2 to 3 e$^-$ *rms*; readout noises of 1 e$^-$ have been achieved but not routinely (Janesick & Elliot, 1992). In sky-limited imaging exposures the field photon noise per pixel >>5 e$^-$; high resolution spectroscopy is the science driver for low readout noise.

- Quantum efficiency – with anti-reflection coatings, thinning, UV flooding etc., ≈70% QE is achievable over a large spectral range, 3000Å– 8500Å, Lesser (1994), though the best recipe remains an art form.

- Dark current – <10 e$^-$ per hour $\rightarrow$ 1 e$^-$ per hour; modern CCDs operated at ≈-110°C have dark currents around 1 e$^-$ per hour, though massive overexposure (daylight) and power cycling effects can increase this by orders of magnitude over periods up to 24 hours later (Tulloch 1995); temperature control also stabilises the temperature -dependent pixel sensitivities. Lower operating temperatures are limited by e$^-$ mobility leading to CTE problems.

- Cosmic ray sensitivity – currently ≈2 events/cm$^2$/minute is the norm. This is usually the limiting factor in the length of individual exposures. Cosmic ray hits can affect many adjacent pixels making effective cleaning from the frame a non-trivial task. Best dealt with by stacking multiple exposures of the field, with the caveat that readout noise is not a problem.

- Dynamic range & linearity – >100,000 e$^-$ full well and linear over this range, ie. a true 16-bit device. Full well depths up to 500,000 e $^-$ are possible, which coupled with a selectable gain (e$^-$ / ADU) enables viable dynamic ranges (peak signal:*rms* noise) between $10^4$ and $10^5$:1 to be regularly obtained.

- Charge transfer efficiency – cumulative CTE's $\gtrsim$0.99999 are now common but the effects of CTE are still readily noticeable downstream of saturated regions where the ambient light level is low. After all, 2048 charge transfers are required to readout an average pixel for a 2048 × 2048 device, resulting in $1 - 0.99999^{2048} = 2\%$ of the total charge left behind as low level charge smears.

• Uniformity – $\lesssim$5% large scale gradient and $\lesssim$1% pixel-to-pixel variations, make subsequent flat-fielding operations much more straightforward. A useful rule-of-thumb is that it is generally feasible to take out 90% of an effect, such as flat-fielding variations, with relatively little effort. To reduce the remainder is often impossible and **always** takes 10 $\times$ the previous effort. Problems occur with thinned CCDs due to the next effect.

• Fringing – target <10% in the I-band; thinned CCDs are prone to fringing particularly toward the red end of the optical spectrum; this is an additive effect, from the viewpoint of analysing images superimosed on the sky, with both spatial (surface properties of the CCD) and temporal components (changing levels of night sky emission lines) and is difficult to reduce to below 1%. Its presence complicates the red-band flat-fielding procedure.

• Defect density – science grade devices should have $\lesssim$1 bad column; $\lesssim$20 bad charge traps. Low light level deferred charge (otherwise known as fat zero, charge skimming, charge depletion and low light level non-linearity) traps were more of a problem in the past but still need checking for in modern devices – see for example Gilliland (1992).

• Miscellaneous – no image retention, cross-talk between read amplifiers and/or different CCDs in mosaic should be minimal, spectral response and gain and bias should be stable over $\approx$week timescales. These latter requirements greatly simplify practical operation of CCDs.

### 3.3. *Availability of CCDs*

Most commercially available CCDs, including those manfucatured by the silcon foundries are made from 4 inch silicon wafers. Some manufacturers have 5 or 6 inch wafer capability but these are at present the exeception rather than the rule. Regardless of wafer size, the maximum physical size of an individual science-grade CCD is limited by the size and purity of currently available silicon wafers to an area of $\approx$ 10–25cm$^2$. The yield of larger science-grade devices is very poor, although non-science grade CCDs covering areas up to 100cm$^2$ have been made. Table 2 lists a sample of the current state-of-the-art CCD suppliers. It is instructive to compare the detective area of these devices with the "industry standard" thinnned TEK 2048 $\times$ 2048 devices currently in use at many observatories. Although the active area has not improved two important changes have occurred: first devices with significantly smaller pixels (with twice as many pixels) are now available; second these new devices can be butted on 3 sides with gaps of less than 1mm between active regions. Because of these changes the next generation of larger area CCD detectors will almost certainly be made from mosaics of individual large format CCDs. This gets around the problems of: low yield; readout limitations; and the physical limitations of the silicon wafers. The papers by Luppino *et al.* (1994) and Boronson *et al.* (1994) describe how mosaic cameras with active arrays of 8192 $\times$ 8192 pixles are being, or have been, constructed using the new "industry standard" 3 edge-buttable 2048 $\times$ 4096 CCD building block. Some of the groups using/constructing mosaic cameras were listed in section 1.4.

### 3.4. *Drift Scanning –v– Point-and-Stare*

Two major methods have been developed for using CCDs in wide field astronomy: drift scanning, eg. Gunn *et al.* (1987), and point-and-stare.

Drift scanning consists of carefully aligning the CCD so that the motion of the sky is exactly along the columns of the CCD and then clocking out the CCD at the same rate/pixel that the sky moves along the columns. Early versions of this technique used a

| CCD | Pixel Size $\mu$ | Format (pixels) | Status |
|---|---|---|---|
| DALSA | 12.0 | 5120 × 5120 | Thick<br>not science grade |
| EEV | 13.5 | 2048 × 4096 | Thick 3 edge-buttable<br>Thinned available soon |
| LORAL | 15.0 | 2048 × 2048 | Wafer runs in foundry |
| | | 2048 × 4096 | Thick 3 edge-buttable<br>Thinning by contract with<br>Lesser – Steward Obs. |
| MIT-Lincoln Labs | ? | 1960 × 2560 | Government funded contract<br>with a consortium of<br>observatories |
| ORBIT | 15.0 | 2048 × 4096 | Wafer runs in foundry<br>Thick 3 edge buttable<br>Thinning ? |
| PHILIPPS | 12.0 | 7000 × 9000 | Thick<br>not science grade |
| RETICON | 13.5 | 2048 × 2048 | Thick buttable ?<br>Thinned ? |
| TEK → SITE | 24.0 | 2048 × 2048 | Thinned packaged<br>Benchmark non-buttable |
| | 15.0 | 2048 × 4096 | Thick 3 edge-buttable<br>Thinned available soon |
| THOMSON | 15.0 | 2048 × 2048 | Thick<br>Thinned ? |

TABLE 2. A Selection of State-of-the-art Large Format CCDs

stationary telescope and let the sky drift past at the sidereal rate, ie. $15cos(\delta)$ arcsec/s, or parked the telescope in declination (easy if equatorially mounted) and tracked at a non-sidereal rate. To minimise the distortion caused by the apparent movement of objects across the CCD, the drift tracks should ideally be along Great Circles in the sky. To see this, consider scanning along the celestial equator as an obvious example of a Great Circle route. Next, as a counter-example, consider declination trackes closer to the celestial poles, where drifting along lines of constant $\delta$ will clearly cause curved tracks across the CCD (imagine star trails near the poles or, if you prefer, consider the locii of lines of constant $\alpha$ or $\delta$ on a tangent plane projection eg. Smart 1956). Any tangent plane projection with a local coordinate track defined by the Great Circle passing through its centre, will provide a minimal distortion route.

The main advantages of drift scanning are:

- large areas of sky can be covered on one frame;
- the continuous readout (after ramping up and down at either end) ensures low overheads;

• the CCD systematic errors (flat-fielding) are reduced to one-dimensional problems, since each pixel in a column contributes equally to the image.

Disadvantages include:

• the problem of aligning and clocking out the CCD to minimise distortion in the output image;
• if the telescope suffers from field distortion (equation 2.23) this will also lead to distorted output images – the SLOAN survey telescope has specially designed corrector plates to remove the field distortion;
• changing observing conditions make it difficult to do precise photometry;
• it is very difficult, if not impossible, to autoguide for large area drift scanning making long exposures too reliant on good telescope tracking. Most drift scanning produces relatively shallow surveys and as such can be well matched to wide field work.

By far the majority of imaging (and spectroscopy) work uses the point-and-stare method with the telescope tracking on the object of interest and an autoguider providing ∼0.1 arcsec position lock. The advantages of this method are:

• simplicity – no complex mechanical platforms are required; optical distortions are readily dealt with;
• all the images are recorded in identical conditions enabling ∼0.1% differential photometry to be routinely achieved;
• autoguiding can be used to give long integration times (up to 1 hour – limited by cosmic ray buildup);
• construction of sky-superflats enables very deep imaging to be obtained by stacking images.

The obvious disadvantages of this method are:

• a much smaller area of sky per exposure is achieved;
• readout overheads can be a significant fraction of short exposure times;
• the full two-dimensional systematics of the CCD have to be dealt with – this is not so much of a problem with modern CCDs where we expect the systematics to start at the 1% level and to be readily reduced to the 0.1% level.

## 4. Preprocessing CCD Images

"The only uniform CCD is a dead one." – Craig Mackay

Since there are many excellent reviews of CCD data processing (see for example, the reviews by Gullixson (1992) and Gilliland (1992); or the NOAO IRAF photometry cookbook), in this section we will concentrate solely on the steps involved in CCD data pre-processing and highlight some of the problems that may be encountered.

The first stage of any reduction of CCD images involves removing the signature of the CCD from the data. This will involve some or all of the following stages:

• Bias frames – provide both an estimate of the artificial zero-point of the digitised images (to ensure non-negative counts) and an estimate of any fixed pattern noise over the frame. The zero-point is usually monitored throughout the observing session by using the overscan region on each frame to keep track of any variation in bias level, and should generally vary by less than 1%. The "trailing" overscan region is generated by continuing

to clock out the CCD after all the charge has been readout and as such solely measures the intrinsic bias level and *rms* noise of the electronics. Note that there is usually an equivalent "leading" underscan region, whose main purpose is to "ramp" up the electronics before real data is read out. Consequently, the overscan region should provide a more reliable estimate of the bias level in the frame. For a modern CCD the bias frame should be a constant, flat level, ie. characterisable by a single number. For an example of unmistakable pattern noise, see figure 9 of Hanisch (1992). If a two-dimensional bias correction is necessary, multiple bias frames need to be taken and combined to remove cosmic ray hits. All other frames are then bias-corrected and overscan regions, underscan regions and any other unwanted strips trimmed off.

• Dark current – the dark current on modern CCDs is usually $\sim$1 $e^-$ per hour and can be ignored. Otherwise, long exposure dark frames are needed to characterise the dark current. As noted earlier, the dark current is both strongly temperature sensitive and power on/off sensitive. The dark frames need to be stacked to remove cosmic-rays and then subtracted off all bias-corrected data frames. The amount to be subtracted is proportional to the relative exposure times. A further advantage of taking a series of dark frames is that the cosmic ray sensitivity can be characterised – useful for optimising cosmic-ray removal routines.

• Flat fields – measure the two-dimensional pixel sensitivity map, including large scale gradients and vignetting caused by dust particles on the filters or CCD window etc.. There are three basic approaches: take dome flats by attempting to uniformly illuminate either the interior of the dome or a white screen using a tungsten light source – hard to get uniform illumination but good for pixel-to-pixel sensitivity measurements; use the twilight sky – problems are short window of opportunity and sky illumination gradients can cause problems for wide field CCDs; make a "superflat" from the astronomical targets using either a shift and add technique, or a series of deep exposures on different regions – not always feasible. Whichever method is used the frames have to be first combined, to remove either cosmic rays or stars/galaxies, before being used to normalise out the sensitivity variations.

• Fringing – an awkward problem with both wavelength and spatial dependence. Only affects thinned CCDs toward red limit of optical spectrum (see previous section). Sky fringing has the added difficulty of being time-varying too, since the relative intensities of the narrow night sky emission lines (ie. those that cause the sky fringing) varies with atmospheric conditions. Continuum sources (eg. most astronomical objects and tungsten dome lamps) are not seriously affected. Note particularly that twilight sky flats will show fringing in the R, I and Z passbands and as such are not suitable for flatfielding the CCD. If fringing is a problem and the dome flats suffer from non-uniform illumination then use the dome flats to remove only the pixel-to-pixel sensitivity variations and use the sky flats to remove the large scale gradients (although even these may be affected by fringing). From the point-of-view of the astronomical objects, the sky fringing is additive, and hence is best estimated and removed by forming a "supersky" by stacking offset target exposures taken under similar atmospheric conditions.

• Cosmic rays – in target frames the effect can be reduced in three generic ways: the optimum method is to modify subsequent analysis programs to ignore them; if this is impractical cosmic-ray removers based on single frames work by varaints on the theme of looking for isolated pixels with intensities/gradients "well above" the local background/gradient – helped by knowledge of the probability distribution function (PDF) of cosmic ray hits (from dark frames) and a good noise model for the detector (readout

noise and photon noise); better is to use multiple frames and perform a pixel-by-pixel comparison using the noise model as previously and some form of k-sigma clipping to reject cosmic rays – see next section.

- Other problems – assorted and include hot spots, traps, dead pixels/columns, saturation, video pattern noise, CTE and smearing, deferred charge etc.. Refer to Gullixson (1992) and Gilliland (1992) and references therein for more details on recognising and dealing with them.

To be a little more precise, we can summarise the various stages of CCD data preprocessing in a compact manner borrowing heavily from the formalism of Gullixson (1992). The raw CCD frame is related to the previous list of corrections by,

$$raw = (obj + sky \times (1 + fringe)) \times qe + dark + flash - skim + bias \tag{4.29}$$

where most of the terms are as above, apart from $flash$, which denotes any pre-flash (low level illumination of CCD using on-board LEDs) that may be applied prior to exposing the CCD in order to reduce the non-linearities caused by deferred charge transfer/skimming, $skim$.

We first correct for the Zero Exposure Additive Spatial Systematics by forming average frames viz;

$$\begin{aligned} < dark > &= dark + flash - skim + bias \\ < skim > &= flash - skim + bias \\ < bias > &= bias \end{aligned}$$

and use the overscan region to monitor and remove variations in bias DC level so that,

$$raw - < .... > -(ovscn - < ovscn >) = (obj + sky \times (1 + fringe)) \times qe \tag{4.30}$$

where $< .... >$ denotes whichever of the 3 corrections or combinations thereof is appropriate or necessary.

To correct for Multiplicative Spatial Systematics, ie. flat fielding, form

$$< flat > = qe + dark + flash - skim + bias \tag{4.31}$$

$$const \times \frac{raw - < .... >}{< flat > - < .... >} = obj + sky \times (1 + fringe) \tag{4.32}$$

where $const$ is a normalising constant chosen to make the average multiplicative $qe$ correction unity.

If fringing is present, or if for some reason the twilight sky flat does not result in "flat" frames, correct for Residual Spatial Systematics – shift and stare and stack, to form

$$< sky > = sky \times (1 + fringe); \quad < sky > = sky \tag{4.33}$$

and either additively apply, if fringing is the cause, or multiplicatively apply if problem was non-uniform flats.

Finally, although this may be necessary in the preceding steps as well, register the individual frames, including geometric distortion corrections as necessary, using variants of the general 6-plate constant linear transformation,

$$x' = a.x + b.y + c; \quad y' = d.x + e.y + f \tag{4.34}$$

and combine. It is simplest to compute the linear transforms by matching the coordinates of pairs of images from each frame. Note that if only shifts are required, $a = 1;\ b = 0;\ d = 0;\ e = 1$; if only a small angle of rotation and shift are required, $a = 1;\ b = -d;\ e = 1$.

### 4.1. *Combining Images*

A common theme in the previous section for both removing the effects of unwanted sources (stars, cosmic-rays etc..) and to improve the signal-to-noise of images, involved combining image frames. Is there an optimum way to do this ? If the frames are aligned astrometrically and scaled photometrically, such that pixels on different frames can be directly combined then the problem is well defined. Otherwise, suitable frame-to-frame transformations as in equation 4.34 need to be applied and possibly some sort of intensity mapping of the form,

$$new = raw \times scale + shift \tag{4.35}$$

to correct for varying sky levels or atmospheric transmission.

Let us now consider a series of matched and scaled values of a particular pixel, with intensities in each of $m$ frames, $x_i$, for $i = 1, m$. For any underlying PDF of the intensities, $P(x)$, which may include contributions from photon noise, readout noise, cosmic rays, bad pixels etc.., various estimators of central location, ie. the "average" value, can be defined. For example:

- the MEAN minimises

$$< (x_i - \hat{x})^2 >_i = \int (x - \hat{x})^2 P(x).dx$$

- the MEDIAN minimises

$$< |x_i - \hat{x}| >_i = \int |x - \hat{x}| P(x).dx$$

- the MODE, or a local fit to the MODE, can be used to estimate the position of the maximum of $P(x)$ but requires an impractically large number of frames to be available.

- If, and only if, $P(x)$ is exactly Gaussian (or Poisson), say with variance $\sigma^2$, is the MEAN the optimum estimator. In which case the error in the "average" values,$\hat{x}$ would be $\sigma/\sqrt{m-1}$. For such idealised cases, the MEDIAN would have error $\sqrt{\pi/2} \times \sigma/\sqrt{m-1}$, but for practical cases would have the added advantage of not being as susceptible to outlying points.

In practice, perfect Gaussian/Poisson distributions are rarely encountered so how do we generalise estimators of central location to cope with "real noise" ?

Tukey and others (Hoaglin, Mosteller & Tukey 1983) have pioneered the development of so-called robust statistics, or m-estimators, to cope with exactly this problem. An m-estimator of central location can be thought of as a way of creating more robust Maximum Likelihood Estimators (MLEs) applicable to "real" noise distributions. Two of the best estimators appear to be Tukey's biweight function and Andrew's wave function. To illustrate the concept, the m-estimators are defined to be the solution of

$$\sum_i \psi(u_i) = \sum_i w(u_i).u_i = 0 \tag{4.36}$$

where $w(u_i)$ can be thought of as a weighting function; $u_i$ is a measure of the relative deviation of the data from the solution

$$u_i = \frac{x_i - T}{c.S} \tag{4.37}$$

with $T$ the best estimate, $S$ the scatter (ie. a measure of the *rms* spread) and $c$ a tuning

constant. In practice equation 4.36 is solved iteratively using

$$\hat{T} = \frac{\sum_i w(u_i).x_i}{\sum_i w(u_i)} \tag{4.38}$$

which at convergence is equivalent to solving equation 4.36 directly. Tukey's biweight function is defined by

$$\psi(u) = u.(1-u^2)^2, \quad |u| \lesssim 1; \quad = 0, \quad |u| > 1 \tag{4.39}$$

and Andrew's wave function by

$$\psi(u) = \frac{1}{\pi} sin(\pi.u), \quad |u| \lesssim 1; \quad = 0, \quad |u| > 1 \tag{4.40}$$

with $S = MAD$ (ie. the Median of the Absolute Deviation from the median, a popular robust estimator of sigma, equivalent to $\sigma_{rms}/0.6745$ for a Gaussian distribution) and $c$ set to between $\approx$6 to 12. Note that both are equivalent to clipping outlying members (cf. k-sigma clipping) from contributing and both perform better than the straight median estimator, whilst remaining robust to aberrant points. For comparison, a k-sigma clipped mean estimator would be specified by $\psi(u) = 1, \quad |u| \lesssim 1; \quad = 0, \quad |u| > 1$.

The condition satisified by equation 4.36 arises naturally from minimising a function of the form

$$\sum_i \rho(u_i); \qquad \frac{d\rho(u)}{du} = \psi(u) \tag{4.41}$$

and suggests a simple equivalence with generalised MLEs. For example: consider a process whereby $x_i = \overline{x} + \epsilon_i$ and the PDF of $\epsilon_i$ is given by

$$P(\epsilon_i) = \alpha.N(0,\sigma_i) + \beta.U(-a,a) \tag{4.42}$$

where $N(0,\sigma_i)$ represents the Gaussian core of the noise distribution, and the uniform distribution, $U(-a,a)$, represents the non-Gaussian extended tail. If the range $[-a,a]$ is large compared to the core size and the fraction of outlying points is low, $\beta << 1$, then to a good approximation this distribution is equivalent to

$$P(\epsilon_i) = \frac{\alpha}{\sqrt{2\pi\sigma_i^2}}.exp(\frac{-\epsilon_i^2}{2\sigma_i^2}), \quad |\epsilon_i| \lesssim k\sigma_i; \quad = \beta, \quad |\epsilon_i| > k\sigma_i; \quad = 0, \quad |\epsilon_i| > a \tag{4.43}$$

or, we could equally well have postulated this form for the PDF at the beginning. Assuming independent measurements, $x_i$, minimising the log-likelihood function then leads to the following estimator for $\hat{x}$,

$$\hat{x} = \frac{\sum_{i=1}^{m'} x_i/\sigma_i^2}{\sum_{i=1}^{m'} 1/\sigma_i^2} \tag{4.44}$$

where $m'$ denotes the observations within the k-sigma clipped range. Equation 4.44 has to be solved iteratively since the clipping boundary is a function of the current estimates of $\hat{x}$ (and $\hat{\sigma}^2$). The well known k-sigma clipping is therefore equivalent to a MLE with a flat extended error tail and illustrates the general applicability of the MLE approach. Note further that equation 4.44 without the k-sigma clipping restriction, is simply the conventional inverse variance weighting scheme, usually derived directly from the requirement that the combined image signal:to:noise ratio should be a maximum. If a more realistic PDF for the non-Gaussian/ Poisson errors is known, including what fraction of pixels are likely to be affected (eg. from the PDF of cosmic rays hits on dark frames), then it is worthwhile considering a numerical solution to the MLE problem that makes direct use of this information.

## 5. Detecting and Parameterising Objects

The previous section dealt with some of the rationale behind removing the detector-dependent signatures from two-dimensional CCD images. We now turn to the problems encountered in detecting and parameterising any objects that may be present in the two-dimensional data. Since, the signature of the detector defines what device was used to create the image, once that signature has been removed, subsequent analysis techniques should be (more-or-less) device independent, ie. applicable to CCD data, digitised photographic data, infra-red array detectors, and so on.

In order to break down the overall analysis strategy into manageable portions the following main tasks can be identified (see Irwin (1985) and references therein for further discussion on these and related points):

($a$) Estimate the local sky background over the field and track any variations at adequate resolution to eventually remove them.

($b$) Detect objects/blends of objects and keep a list of pixels belonging to each blend for further analysis.

($c$) Parameterise the detected objects, ie. perform astrometry, photometry and some sort of shape anaylsis.

In deciding on a rationale for these three stages, natural questions to consider are: is it feasible to do the whole analysis automatically – after all wide field optical astronomy has the potential to generate Gbytes of data per night; how does a human observer interactively interpret two-dimensional maps and what can we learn from this; how accurate are any derived image parameters likely to be; and closely related to this last question, which methods of analysis will give the best results at reasonable computational cost ?

### 5.1. *Sky Background Analysis*

To track any potential background variation, the whole field can be partitioned up into an array of suitably-sized "background regions". (Here, suitable means, a compromise between small enough size to follow real variations and large enough size to reduce subsequent error in the estimate.) For each region compute the pixel intensity histogram and derive various statistics from it, as illustrated in figure 9. A straight mean is clearly hopeless, since even in regions free of faint objects, the odd pixel defect can be enough to seriously bias it. The median is a significant improvement, but owing to the innate skewness of the histogram will always tend to overestimate the local sky level. A popular method, and one which I recommend, is to fit a Gaussian to the core (ie. within say $\pm 1$ sigma) of the histogram, as a robust estimator of the mode, an esimate of sigma is a useful byproduct. This works well in relatively uncrowded regions but again systematically overestimates the sky level as the image number density goes up (see Irwin (1985) for examples). Finally, modelling the skewness of the histogram explicitly (Bijaoui, 1980) can in principle give the most unbiassed answer, although unfortunately the strong correlation between the asymmetry in the data (usually a free-parameter in the model) and the sky location can lead to instability problems.

A problem with histogram methods, particularly with full 16-bit data, is selecting a sensible bin size – too fine a sampling and the mode is ill-defined; too coarse and resolution is lost due to quantisation. A useful rule of thumb is to select a bin size such that the noise level at sky, $\sigma_{sky} \approx 10$ units. Gaussian fitting to the modal core region can readily recover information at a 1/10th bin size level. This is usually much smaller than either the systematic errors caused by contaminating objects, or the random error in the sky estimate $\approx N_{pixels}^{-1/2} \times \sigma_{sky}$; where $N_{pixels}$ is the number of pixels in the histogram within $\pm 1\sigma_{sky}$ of the sky level.

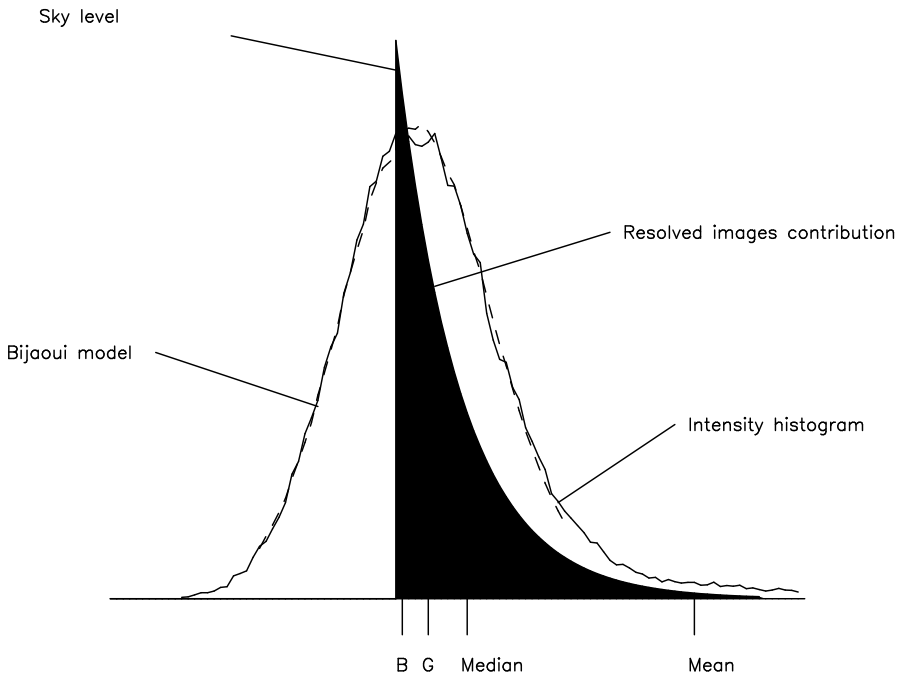


FIGURE 9. Sky background estimation from assorted statistics of the pixel intensity histogram. The histogram of the shaded region is convolved with the PDF of the noise to give the observed intensity distribution. Note in particular how the most widely used estimators of sky level are ordered: Mean > Median > mode (from Gaussian fit - G) > Bijaoui model fit (B), due to the skewness caused by resolved images. A popular variant, the k-sigma clipped mean computed directly from the data, can be as good as the Gaussian fit to the mode.

---

Combining all the background region sky estimates then gives a two-dimensional array of "background" values that can be further processed to help remove regions affected by, for example, the halos of bright stars or galaxies. A local sky value at any point in the original field can then be obtained by interpolation from the background array. This is the approach adopted by the APM facility in automatically processing photographic plates (see Kibblewhite *et al.* , 1984 and Irwin & Trimble, 1984). Note that the process of estimating the background, or sky level, has been completely decoupled from estimating the parameters of an object.

The preceding approach can be thought of as a variant on the scheme of digitally filtering the full two-dimensional pixel map to remove "slowly varying" features, ie. background variations. A popular alternative based on this analogy, is to use something like a two-dimensional median filter (Tukey, 1971) followed by a linear filter (to reduce the step-like appearance median filtering leaves behind), to track the slowly varying features. These are then subtracted off to leave a sky-less map. This method itself is of course a variant of unsharp-masking (eg. Pratt, 1978).

A final alternative is to estimate the background on an image-by-image basis (eg. Newell, 1982). To do this, define an "annulus" around each image, with inner radius several psf radii away, and an outer radius as large as possible. Within the annulus

compute either a k-sigma clipped mean estimate, or use the modal estimator $mode = 3 \times median - 2 \times mean$. The latter formula is a good working approximation for a generalised Gaussian distribution of the form N(0,1) $\times(1 + \alpha.(x^3 - 3x))$, but I would recommend the clipped mean because of its generality.

There are three main problems with the image-by-image method. First, setting appropriate annulii boundaries when dealing with mixtures of stars and galaxies of unknown profile (plus the problems of neighbouring images), is non-trivial. Second, although the combination of spatial clipping, inherent in the annulus approach, and intensity clipping seems like an improvement on the histogram, remember that the psf of star images is much larger than a few core radii and it is precisely these same low level, but large area, intensities near sky, that cause the trouble with either the k-sigma clipping algorithm or the histogram method. A final criticism, is that while a histogram-based method attempts to make full use of all the pixel information and the continuity of the background values, this is not true of the local image method.

### 5.2. *Optimal Detection of Images*

The classical approach for optimum detection of signals (images) in the presence of random noise is to apply a matched detection filter to the raw data prior to setting detection criteria (see for example Pratt, 1978). To a good approximation the random noise present on the detector comes from a Gaussian/Poisson process and is easy to deal with. However, the presence of other images in the data, particularly faint stars and background galaxies, and possible systematic artefacts due to the detector, complicates things by introducing a "systematic" noise component. Here we define any artefact/image outside of the image of interest, to be a potential systematic noise problem. A good example of this arises in the problem of detecting Low Surface Brightness Galaxies (LSBGs). Since LSBGs often have scale sizes of $\approx$1 arcmin, multitudes of other faint images will generally be superimposed and make the identification task more complex.

Woodward & Davies (1958) presented a useful insight to the problem of optimal detection of images using a straightforward application of Bayes' theorem. The argument runs as follows: consider the question of detecting the reflected echo of a radar pulse of known shape, $x_{t+\tau}$, but unknown lag $\tau$, buried within a noisy, discretely sampled, time series, $y_t$, such that

$$y_t = x_{t+\tau} + \epsilon_t \tag{5.45}$$

where $\epsilon_t$ is assumed to be random Gaussian noise of variance $\sigma_t^2$ †. The aims are to locate the signal and in doing so accurately estimate the position, $\tau$. We first construct the likelihood function of observing the sequences, $x_t, y_t;\ t = 1, ....N$, for a particular value of $\tau$,

$$L(\mathbf{x}, \mathbf{y} \mid \tau) = \prod_{t=1}^{N} P(\epsilon_t \mid \tau) \tag{5.46}$$

and then use Bayes' theorem to argue that in the absence of prior information, finding the maximum of the likelihood function is equivalent to finding the most probable value of $\tau$ given $\mathbf{x}$ and $\mathbf{y}$. Now

$$P(\tau \mid \mathbf{x}, \mathbf{y}) \propto exp(-\sum_{t=1}^{N} \frac{\epsilon_t^2}{2\sigma_t^2}) \tag{5.47}$$

† It is straightforward to generalise to non-independent noise using a generic multivariate Gaussian distribution, which leads to a "least-squares" estimator based on a Mahanoublis metric.

and maximising the probability is equivalent to a weighted least-squares minimisation of

$$\sum_t \frac{\epsilon_t^2}{\sigma_t^2} = \sum_t \frac{1}{\sigma_t^2}.(y_t - x_{t+\tau})^2 \tag{5.48}$$

or in the case of $\sigma_t^2 = constant$, finding the maximum of the cross- correlation of $y_t$ with $x_{t+\tau}$. Not only does this illustrate how a cross-correlation function is related to the solution we seek, it shows how to generalise the traditional cross-correlation approach to deal with more complex forms of noise contamination.

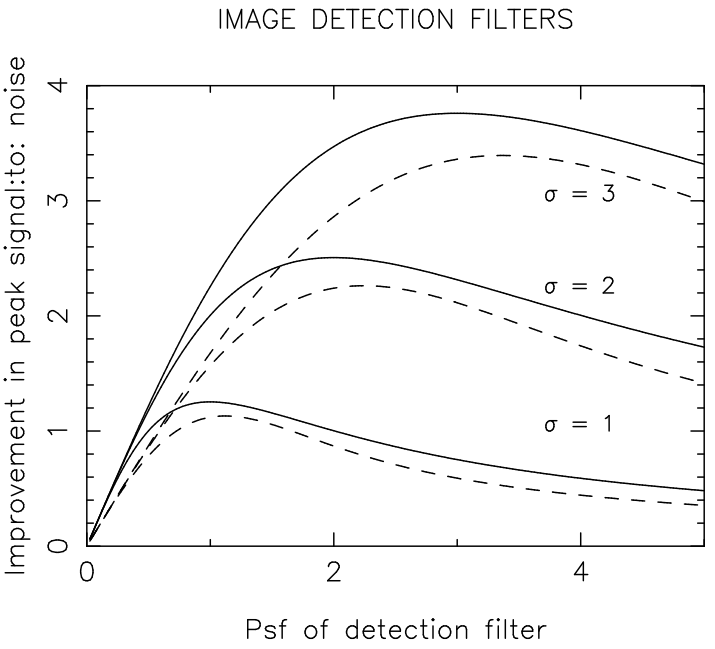


FIGURE 10. Performance of various detection filters for target Gaussian images of $\sigma = 1, 2, 3$. Solid lines are for Gaussian filters and dashed lines are for circular top-hat filters. Note: how the improvement peaks for filters of equivalent scale size to the target objects; how insensitive the improvement is to the exact size of the filter; and how insensitive the performance is to the exact shape of the filter.

---

To go back to our original problem of detecting images in noise; since the only images difficult to locate are those marginally above the sky noise, a constant noise approximation is a valid assumption and certainly for a CCD, the noise in adjacent pixels is to all intents and purposes random. In other words, to optimally detect images, cross-correlate † the entire frame with the appropriate filter; the psf in the case of point-like sources and possibly an exponential function of chosen scale length for larger faint galaxies.

From a practical viewpoint a matched filter maximises the resultant peak signal:to:*rms*

† This is the same operation as convolution for symmetric profiles – desirable since they induce no systematic shift in image position. Most detection filters are also normalised to unit area under the curve, to ensure average intensities remain the same.

noise. The same criteria can indeed be used to derive it. Figure 10 illustrates this improvement for a series of Gaussian target objects using both Gaussian and top-hat detection filters of various sizes. Defining the two-dimensional target profile as $I = I_p.exp(-r^2/\sigma^2)$ and the normalised detection filter as $I = exp(-r^2/\sigma_g^2)/\pi\sigma_g^2$ changes the peak intensity, $I_p \rightarrow I_p \div (1 + \frac{\sigma_g^2}{\sigma^2})$, and changes the noise, $< \epsilon^2 > \rightarrow < \epsilon^2 > \div \sqrt{2\pi\sigma_g^2}$. A similar exercise can be carried through for normalised circular top-hat filters of radius, $a$, to show that the improvement becomes $\sqrt{\pi a^2} \times \sigma^2/a^2 \times exp(-a^2/\sigma^2)$. Because the performance gain in peak signal:to:*rms* noise is relatively insensitive to the exact size and shape of the filter, it is then feasible to use non-linear variants of the preceding filters to detect large LSBGs in the presence of contaminating foreground/background objects. See Irwin *et al.* (1990) for more details and examples of the galaxies detected.

### 5.3. *Detecting Using Pixel Connectivity*

The main purpose of the detection filter is to enhance the peak signal:to:noise to optimise the performance of object locating algorithms. Most of these algorithms are some variant on the theme of peak (eg. Herzog & Illingworth, 1977) or island searches (eg. FOCAS – Tyson & Jarvis, 1979). Both methods work by first prescribing a pixel detection threshold above background, otherwise known as a detection isophote, and then proceed to look for either isolated peaks, or islands of contiguous pixels above this threshold. Since most peak-based methods examine the intensities of neighbouring pixels too, there is in practice, little difference between the two approaches and I will stick to describing the pixel connectivity approach.

Figure 11 illustrates the main concepts. Potential images are defined as regions of simply-connected pixels above the detection isophote, relative to the local sky background. Two passes through the data are recommended. On the first pass the sky background is estimated, as outlined previously, and on the second pass the sky level (interpolated if necessary) plus the threshold, define those pixels that require further examination. Spurious images or noise are rejected using a combination of the requirements for a pixel to be above threshold and for it to be connected with enough neighbours to meet a chosen minimum size criterion. The threshold is usually set to be some fixed multiple ($\approx$2) of sky noise above sky. Once a potential image has been located, the original pre-detection filter intensities of the pixels are used for subsequent analysis. This latter requirement ensures that any derived image parameters are unaffected by the blurring action of the detection filter. Of the two most commonly used isophotal connectivity paths, the four nearest neighbour route (N,S,E,W) seems to give better performance than the eight-fold neighbour approach (N,S,E,W + NW,SE,NE,SW). The latter type of connectivity tends to produce more spurious pixels in the outer parts of an image leading to somewhat noisier image parameters.

The operations required to do all this, using only one pass through the data and minimal memory requirements, ie. enough rows of pixels in memory to do the detection filtering, can be summarised as follows (see Lutz, 1979 for more details):

(*a*) Set up parent, link-list and pixel information arrays/stack. The parent list, a label for potential new images, points to the position of the 1st link in the link-list for this image; the link-list entry then points to the next pixel for this image and so on; while the pixel information arrays store the i,j position and original intensity of the pixel in the location specified within the link-list.

(*b*) Read in a new row of pixels; do filtering and save original intensities. The filtering is of necessity out of phase with the row of data currently being analysed for objects.

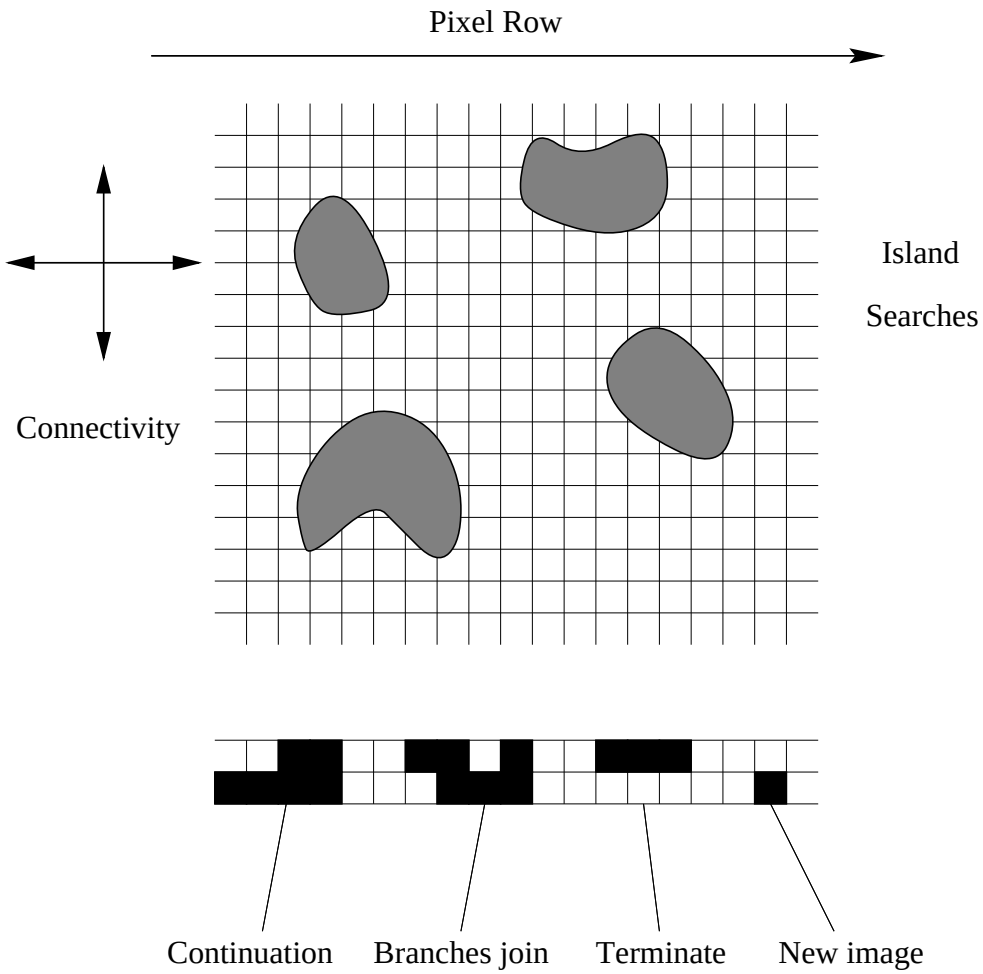


FIGURE 11. The basis of pixel connectivity algorithms

(*c*) Set the background level and add on threshold and flag pixels above this level.

(*d*) Is pixel i,j neighbour to any active pixels in the current parent/link lists or not ? It must be either: a continuation of an image to add to the linked-list; a joining of two branches of previously separate images (see figure 11) requiring updates of parent and link-list arrays; or a potential new image.

(*e*) If within a row no pixels join to a previously active parent image, terminate that image, process pixels to generate parameters and return free slots to stack.

### 5.4. *Estimating Image Parameters*

The isophotal connectivity method of the previous section only makes use of the information stored in those pixels that passed the threshold and contiguity criteria. The advantages of this approach are that it is computationally fast and straightforward to implement; and that a wide variety of useful and robust image parameters can be derived. The following list demonstrates the range of typical image parameters that can be computed from the connected pixel list in a single pass. These are the image parameters

that are widely used by the measuring machine community for astrometry, photometry and image shape description (see for example MacGillivray & Stobie, 1985). It is worth stressing that a single photographic Schmidt plate, the raw material for the measuring machines, contains up to 4 Gbytes of data, recorded in a highly non-linear fashion, and that the currently available sky surveys total well over 20 Tera-bytes of data. The ability to process large volumes of data quickly is also highly relevant for processing wide field CCD data. Examples of alternative strategies, usually involving significantly more computational effort, will be given in the next section. In all the following equations, $I(x_i, y_i)$ denotes the intensity of the ith pixel found in the island search phase and the sum is over all detected connected pixels. We shall assume for simplicity that all detected images are single objects. For more details on dealing with overlapped blended images see Irwin (1985).

Isophotal Intensity – the integrated flux within the boundary defined by the threshold level; ie. 0th moment

$$I_{iso} = \sum_i I(x_i, y_i) \tag{5.49}$$

For Gaussian images, this is related to the total intensity by the factor $(1 - I_t/I_p)^{-1}$, where $I_p$ is the peak flux and $I_t$ the threshold level relative to sky. This implies that for images close to the detection limit, $I_p \approx I_t$, isophotal magnitudes will be around 1 magnitude fainter than total magnitudes.

Position – computed as an intensity-weighted centre of gravity; ie. 1st moment

$$x_o = \sum_i x_i.I(x_i, y_i) / \sum_i I(x_i, y_i) \tag{5.50}$$

$$y_o = \sum_i y_i.I(x_i, y_i) / \sum_i I(x_i, y_i)$$

Note that the intensity weighting and the isophotal connectivity criteria automatically reduce the sensitivity of the estimator to outlying points.

Covariance Matrix – the triad of intensity-weighted 2nd moments is used to estimate the eccentricity/ellipticity, position angle and intensity-weighted size of an image

$$\sigma_{xx} = \sum_i (x_i - x_o)^2.I(x_i, y_i) / \sum_i I(x_i, y_i) \tag{5.51}$$

$$\sigma_{xy} = \sum_i (x_i - x_o).(y_i - y_o).I(x_i, y_i) / \sum_i I(x_i, y_i)$$

$$\sigma_{yy} = \sum_i (y_i - y_o)^2.I(x_i, y_i) / \sum_i I(x_i, y_i)$$

The simplest way to derive the ellipse parameters from the 2nd moments is to equate them to an elliptical Gaussian function having the same 2nd moments. It is then straighforward to show (eg. Stobie, 1980) that the scale size, $\sqrt{\sigma_{rr}}$, is given by, $\sigma_{rr} = \sigma_{xx} + \sigma_{yy}$; the eccentricity, $ecc = \sqrt{(\sigma_{xx} - \sigma_{yy})^2 + 4.\sigma_{xy}^2}$ / $\sigma_{rr}$; and the position angle, $\theta$ is defined by, $tan(2\theta) = 2.\sigma_{xy}/(\sigma_{yy} - \sigma_{xx})$. Higher order moments have been used as shape descriptors (eg. Tyson & Jarvis, 1979), but are generally much more prone to corruption by outlying noisy data pixels.

Areal Profile – an interesting variant on the radial profile, which measures the area of an image at various intensity levels. Unlike the radial profile, which needs a prior estimate of the image centre, the areal profile provides a single pass estimate of the

profile

$$Areal\ Profile\ \rightarrow\ \ T+p_1, T+p_2, T+p_3, .....T+p_m \tag{5.52}$$

where $p_j; j = 1, ...m$ are intensity levels relative to the threshold, $T$, usually spaced logarithmically to give even sampling.

The peak height, $I_p$, is a useful related addition to the areal profile information and is defined as

$$I_p = max[I(x_i, y_i)]_i \tag{5.53}$$

or alternatively measured by extrapolation from the areal profile if the image is saturated (straightforward for photographic plates, but charge leakage causes problems with CCD data).

Other useful measures of image size are those defined by Kron (1980) based on moments of the radial profile.

$$r_1 = \int r.I(r)dr / \int I(r)dr; \quad r_{-2} = \int r^{-2}I(r)dr / \int I(r)dr \tag{5.54}$$

These involve more than one pass through the data but are good shape discriminators for morphological classification. There are many other methods of parameterising the shape information as the front end to an object classification scheme (eg. star/galaxies/noise). A recent review of the field is given by Odewahn (1995).

## 6. Alternatives Methods for Astrometry and Photometry

Maximum likelihood theory enables us to devise optimum methods for estimating image parameters and also specifies the minimum attainable error it is possible to achieve for images of a given profile and signal:to:noise (eg. Irwin, 1985). Isophotal methods are not generally optimal, but they are robust, require no prior knowledge of the image profile, and are simple to compute. A serious drawback in their direct use is that the derived intensities are biased, since a varying fraction of the total flux is included. Although there are assorted tricks to get around this problem for stellar images (eg. Bunclark & Irwin, 1983), recovering the lost flux for an unknown galaxy profile is more difficult. From an information-theoretic viewpoint the loss of information in neglecting the outer parts of the profile is not so serious, since most of the information regarding image location and total intensity comes from the higher signal:to:noise inner part of the profile. Consequently, bias notwithstanding, isophotal methods actually come quite close, certainly within <50%, of the minimum attainable error bound.

In principle, a stellar image is completely specified by its coordinates and intensity. In practice, variations in psf across the field and lack of prior knowledge about which images are stellar conspire to make life more complicated. The problem is much worse for galaxies, since we have no prior knowledge of their profile. These problems have lead to a whole range of methods, particularly photometric methods, to circumvent the lack of knowledge.

### 6.1. *Aperture Photometry*

There are two basic approaches for estimating total intensities. The first is to integrate the flux within an aperture. The second is to fit some sort of profile to the image and then renormalise the profile-based intensity to be equivalent to a total one. Apertures are either fixed in size (usually for bright stellar photometry only) or allowed to "grow" automatically out to some pre-specified maximum area.

Aperture photometry is defined by

$$I_{ap}(r) = \sum_{i}^{N} I_i - N \times sky \tag{6.55}$$

such that all pixels indexed by $i$ are within a radius, $r$, of the image centre †. An isophotal estimate of the image centre, as in equation 5.50, is usually adequate. Intensity contributions from pixels crossing the boundary are usually added in on a pro-rata basis. Defining $I_i$ to be the object flux + sky flux in pixel $i$, clarifies the dependence of $I_{ap}(r)$ on the accuracy of the sky estimate – assumed constant over the image. The problem with aperture photometry is the necessary tradeoff between capturing all the light, = large radius; adding in too much sky noise = $\sqrt{N} \times \sigma_{sky}$; and being mislead by systematic errors in the sky level = $N \times \Delta_{sky}$. The usual approach to minimise these problems is to "examine" the curve-of-growth, $I_{ap}(r)$ -v- $r$, as illustrated in figure 12. Another problem, not shown in the figure, is the presence of neighbouring images, which will also lead to an upturn in the curve. In this example, the systematic errors in the sky estimate correspond to $\pm 1\%$ errors in the absolute sky level for a typical scale length galaxy image at a similar magnitude to a 1 arcsec$^2$ patch of sky. Figure 2. of Irwin (1985) shows how typical estimators of sky can readily be off by 1% in even moderately crowded fields.

For stellar images, assuming the psf does not vary rapidly around the field, it is possible to minimise the preceding problems by calibrating the curve-of-growth using isolated bright stellar images. Fainter stars can then be integrated out to a compromise radius (usually a few core radii) and then a well defined correction applied. Clearly this is not possible for galaxy images and some sort of empirical fit to the curve-of-growth (eg. 3rd order polynomial and look for zero derivative out to some maximum radius) seems to be as good a method as any of automating the decision and minimising the effects of sky noise (see Irwin & Hall (1982) for more details).

### 6.2. *Profile Fitting*

Profile fitting, usually limited to stellar images, is now well served by several software packages such as: ROMAFOT – Buonanno & Iannicola (1989); DoPHOT – Mateo, Saha & Schecter (1990); and DAOPHOT – Stetson (1987). These references address the main problems and issues involved in successful profile fitting; whilst the work by King (1983), Irwin (1985) and Goad (1986) investigates the theory underpinning optimal fitting and shows how this can be used to predict the likely errors of the derived parameters. Stellar psf fitting is the only reliable technique to use in crowded regions such as those found toward the centre of globular clusters. By iterative use of difference maps (data – psf model) and by simultaneous fitting of overlapping components in a blended image, results very close to the theoretical error bound can be achieved.

Very briefly, the main decisions to be made in profile fitting are:

(*a*) is the profile, ie. psf, adequately constant across the frame or does some allowance for geometric variation need to be folded in (eg. HST data; ROSAT data) ?

(*b*) can the psf be approximated using an analytic function ? Usually some mixture of Gaussian-exponential-Lorentzian or a Moffat profile, $(1 + r^2/a^2)^{-\beta}$, are used.

(*c*) if the images are noticeably trailed is an elliptical deformation of one of the above profiles adequate ? or,

(*d*) does an empirically constructed profile need to be formed from isolated stars ? If the seeing psf is not well sampled then some sort of sub-pixel interpolation will be

† Elliptical apertures, parameterised by semi-major axis radius, were used by Irwin & Hall (1982) for galaxy photometry to minimise the area of sky included.

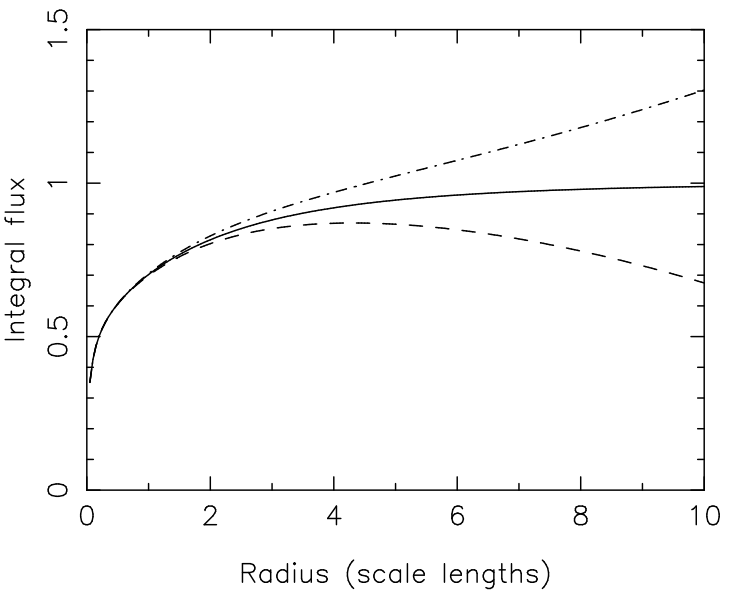


FIGURE 12. Idealised curves-of-growth for aperture integration of an exponential profile. If the sky level is exactly correct, $I_{ap}(r)$ will asymptotically stabilise to the desired level. If the sky estimate is too high the curve will turn over (dashed), too low and the curve continues rising (dot-dash). The effect of noise in the data is not shown.

necessary to reconstruct the model profile at non-integral pixel locations. This is easy with analytic profiles, harder for empirical profiles.

(*e*) how large a region around each image should the psf be fitted over ? With a complex blend of several images this is not necessarily straightforward to answer. A simple solution is to only use those pixels picked out by some isophotal detection algorithm.

(*f*) should a local estimate/update for the background level, caused by unresolved images etc., be made simultaneously with the psf parameter fitting ?

(*g*) if the profile is an exact match for the psf, total intensities = profile intensities. In practice this is rarely the case and isolated bright stars are used to estimate the offset between the profile and total intensity systems.

For more details on these and other points consult the preceding references.

There is a very simple link between isophotal intensity estimation and profile fitting for isolated images, which goes some way to show why isophotal estimates are so popular. With the usual Gaussian/Poisson noise encountered in optical work, all profile fitting methods reduce to weighted least-squares methods of the form of minimising

$$F = \sum_i \frac{(d_i - m_i)^2}{\sigma_i^2} \tag{6.56}$$

where $d_i$ and $m_i$ are respectively the data and model at pixel $i$, and $\sigma_i^2$ is the expected

noise variance $< \epsilon_i^2 >_i$, such that $d_i = m_i + \epsilon_i$. † For a single profile, with assumed known position, $m_i = k.\phi_i$, where $k$ is the unknown scaling factor and $\phi$ is the normalised psf (ie. $\int\int \phi(x,y)\ dxdy = 1$ ) shifted to the appropriate location. Solving for the intensity parameter then gives

$$k = \frac{\sum_i \phi_i.d_i/\sigma_i^2}{\sum_i \phi_i^2/\sigma_i^2} \tag{6.57}$$

which is nothing more than a weighted sum over the pixel intensities belonging to the image , although subtle differences between the data–model overlap integral in the numerator, and the model–model overlap integral in the denominator, are the cause of the intensity renormalisation problem mentioned previously. There are two interesting limiting cases: for bright images well above sky, Poisson noise dominates, so that $\sigma_i^2 = \phi_i$ (if the gain is unity, $\propto$ otherwise) and the profile intensity is simply $\sum_i d_i$, the isophotal intensity; for a faint image dominated by constant sky noise the profile intensity is just the profile-weighted sum of the pixel intensities. This analogy can be extended to multiple overlapping images, using more complex weighting factors.

### 6.3. *Astrometry – Image Centering*

In the late 1970's the most popular method for locating the centre of an image involved using marginal sums of the image intensity distribution. This reduces a two-dimensional problem to a pair of one-dimensional problems, with subsequent savings in computer time. The marginal sum method involves some variant along the lines of the following steps. First, form $\rho(x_i)$, and equivalently $\rho(y_i)$, where

$$\rho(x_i) = \sum_{j=-a}^{j=+a} I_{i,j} \tag{6.58}$$

and then find the centre of the one-dimensional distribution(s) using either: the median, a Gaussian fit to the distribution (often including a sloping background component rather than a constant), or a variant of the centre of gravity such as

$$\bar{x} = \frac{\sum_i [\rho(x_i) - \bar{\rho}].x_i}{\sum_i [\rho(x_i) - \bar{\rho}]} \tag{6.59}$$

using only those pixels with $\rho(x_i) \gtrsim \bar{\rho}$. Iterate through these two steps if $\bar{x}$ is more than 1 pixel from the window centre. Although computationally fast, there are several shortcomings of the method: the window has to be centred fairly accurately to start with or the iterative solution can diverge; neighbouring images can corrupt the marginal distribution and bias the answer away from the true centre; if the window $[-a, a]$ is too large excessive noise is folded in, too small and much of the information is lost. Irwin (1985) outlined how this potential loss of information degrades the performance of the algorithm and suggested ways of minimising the problem by using Maximum Likelihood theory to establish the optimum window to use.

In many ways, the marginal sum method was superceded by the centre-of-gravity estimates derived from pixel connectivity algorithms – ie. isophotal centre-of-gravity estimators such as equation 5.50. If we generalise such an estimator to include a weighting term, $w_i$, (cf. equation 6.57 for intensity estimation) along the lines of

$$\bar{x} = \frac{\sum_i w_i \times x_i \times I_i}{\sum_i w_i \times I_i} \tag{6.60}$$

† For those condemned to work with few photons per resolution element, as is often the case in X-ray or $\gamma$-ray astronomy, the equivalent expression is, $F = \sum_i d_i.ln(m_i) - m_i - ln(d_i!)$.

where the summation is over all isophotally connected pixels, is there an optimum weighting factor ? Put another way, what does Maximum Likelihood theory suggest ? For an image with underlying normalised profile, $\phi(x,y)$, the optimum weight is given by

$$w_i = \left[\frac{1}{x-\bar{x}} \times \frac{\delta\phi}{\delta x}\right]_i \times \frac{1}{\sigma_i^2} \tag{6.61}$$

Clearly, this involves an iterative solution for $\bar{x}$ (and $\bar{y}$). Irwin (1985) shows how to extend this scheme to overlapping blended images.

As an example, for a radially symmetric Gaussian profile, this simplifies to $w_i \propto \phi(x_i,y_i)/\sigma_i^2$. As in the previous section, the two limiting cases are very revealing. For bright images, $w_i$ is a constant, implying that for such cases isophotal centre-of-gravity methods are close to optimal. For faint images, $w_i \propto \phi(x_i,y_i)$, and profile weighting, with iteration, is the answer.

For more details of the derivation of optimum estimators and a full error analysis see the papers by, King (1983), Irwin (1985) and Goad (1986).

## 7. Acknowledgements

In preparing the section on telescope optics I have benefited from many fruitful conversations with Roderick Willstrop and Ian Parry and would like to thank them for their help. I am also indebted to Richard McMahon for letting me borrow from his notes of sky surveys in other wavebands. Finally I would like to acknowledge the financial support provided by the Instituto de Astrofisica de Canarias, and to thank them for inviting me to take part in the Winter School.

## REFERENCES

Becker, R.H., White, R.L. & Helfand, D.J., 1995, *Astrophys. J.,* **450**, 559.

Bijaoui, A., 1980, *Astr. Astrophys.,* **84**, 81.

Boksenburg, A., 1972, in *Proceedings of the ESO-CERN Conference on Auxiliary Instrumentation for Large Telescopes*, eds. S. Lausen & A. Reiz, 295.

Boronson, T., Reed, R., & Wong, W.Y., 1994, in ....., Proc. SPIE, **2198**, 877.

Bradt, H.V.D., Ohashi, T., & Pounds, K.A., 1992, in *Ann. Rev. Astron. Astrophys.*, **30**, 391.

Buonanno, R., & Iannicola, G., 1989, *Publ. astr. Soc. Pacific,* **101**, 294.

Bunclark, P.S., & Irwin, M.J., 1983, in *Proc. Statistical Methods in Astronomy*, ESA SP-201, 195.

CFHT MOCAM User Manual, 1995.

Dainty, J.C. & Shaw, R., 1974, in *Image Science*, Academic Press.

Demers, S., Kibblewhite, E.J. Irwin, M.J., Nithakorn, D.S., Beland, S., Fontaine, G., & Wesemael, F., 1986, *Astr. J.,* **92**, 878.

Fisher, R.A., Corbett, A.S., & Williams, C.B., 1943, Journal of Animal Ecology, **12**, 42.

Fordham, J.L.A., Bone, D.A., Michel-Murillo, R., Norton, T.J., Butler, I.G., & Airey, R.W., 1994, in ....., Proc. SPIE, **2198**, 829.

Geary, J.C., Luppino, G.A., Bredthauer, R., Hlivak, R.J. & Robinson, L., 1991, *Proceedings of The SPIE: CCDs and Solid State Optical Sensors II*, .....

Gilliland, R.L., 1992, in *Astronomical CCD Observing and Reduction Techniques*, ed. S.B.Howell, ASP Conf. Series, Vol. 23, 68.

Gilmore, G., & Walton, N., 1993, *Gemini*, **40**, 16.

Goad, L., 1986, in *Instrumentation in Astronomy*, SPIE Vol. **627**, 688.

Gullixson, C.A., 1992, in *Astronomical CCD Observing and Reduction Techniques*, ed. S.B.Howell, ASP Conf. Series, Vol. 23, 130.

Gunn, J.E., *et al.* , 1987, *Optical Engineering*, **26**, 779.

Hanisch, R.J., 1992, in *Astronomical CCD Observing and Reduction Techniques*, ed. S.B.Howell, ASP Conf. Series, Vol. 23, 285.

Hartley, M., 1994, in *Digitised Optical Sky Surveys* , eds. H.T.MacGillivray and E.B. Thomson, Kluwer Academic Publishers, Dordrecht, p.117.

Herzog, A.D., & Illingworth, G., 1977, *Astrophys. J. Suppl.,* **33**, 55.

Hoaglin, D.C., Mosteller, F., & Tukey, J.W., 1983, *Understanding Robust and Exploratory Data Analysis*, Wiley, Chp 11.

Irwin, M.J., & Hall, P., 1982, *Occ. Repts. R. Obs. Edin.*, **10**, 111.

Irwin, M.J., & Trimble, V., 1984, *Astr. J.,* **89**, 83.

Irwin, M.J., 1985, *Mon. Not. R. astr. Soc.,* **214**, 575.

Irwin, M.J., Davies, J.I., Disney, M.J., & Phillipps, S., 1990, *Mon. Not. R. astr. Soc.,* **245**, 289.

Irwin, M.J., 1992, in *Digitised Optical Sky Surveys* , eds. H.T.MacGillivray and E.B. Thomson, Kluwer Academic Publishers, Dordrecht, p.43.

Irwin, M.J., 1994, in *Working Group on Wide Field Imaging – Newsletter No. 5*, 25.

Janesick, J., & Elliot, T., 1992, in *Astronomical CCD Observing and Reduction Techniques*, ed. S.B.Howell, ASP Conf. Series, Vol. 23, 1.

Jorden, P.R., Deltorn, J., & Oates, A.P., 1994 in ....., Proc. SPIE, **2198**, 836.

Kibblewhite, E.J., Bridgeland, M.T., Bunclark, P.S., & Irwin, M.J., 1984, in *Proc. Astronomical Microdensitometry Conference*, NASA-2317, 277.

King, I., 1983, *Publ. astr. Soc. Pacific,* **95**, 163.

Kron, R.G., 1980, *Astrophys. J. Suppl.,* **43**, 1.

Kron, R.G., 1995, *Publ. astr. Soc. Pacific,* **107**, 766.

Lasker, B.M., 1995, in *Future Utilisation of Schmidt Telescopes*, IAU Symposium No. 148, eds. R.D.Cannon *et al.* , ASP, San Francisco (in press).

Lasker, B.M., 1995b, *Publ. astr. Soc. Pacific,* **107**, 762.

Lesser, M.P., 1989, in *CCDs in Astronomy*, ed. G.H. Jacoby, ASP Conf. Series, Vol. 8, 65.

Lesser, M.P., 1994, in ....., Proc. SPIE, **2198**, xxx.

Luppino, G.A., Bredthauer, R.A., & Geary, J.C., 1994 in ....., Proc. SPIE, **2198**, 810.

Lutz, R.K., 1979, ..... 213.

MacGillivray, H.T., & Stobie, R.S., 1985, in *Vistas in Astronomy*, **27**, 433.

Mateo, M., Saha, P., & Schecter, P., 1990, DoPHOT Users Manual.

Morgan, D.H., 1995, in *Future Utilisation of Schmidt Telescopes*, IAU Symposium No. 148, eds. R.D.Cannon *et al.* , ASP, San Francisco (in press).

Newell, E.B., 1982, *Occ. Repts. R. Obs. Edin.*, **10**, 111.

Odewahn, S.C., 1995, *Publ. astr. Soc. Pacific,* **107**, 770.

Parker, Q.A., Philipps, S., Morgan, D.H., Malin, D.F., Russell, K.S., Hartley, & Savage, A., 1994, in *Astronomy from Wide-Field Imaging*, IAU Symposium No. 161, eds. H.T.MacGillivray *et al.* , Kluwer Academic Publishers, Dordrecht, p.129.

Pratt, W.K., 1978, *Digital Image Processing*, Wiley.

Prestage, R., & Peacock, J., 1983, *Mon. Not. R. astr. Soc.,* **204**, 355.

Price, S., 1988, *Publ. astr. Soc. Pacific,* **100**, 171.

Russell, K.S., Malin, D.F., Savage, A., Hartley, M. & Parker, Q.A., 1992, in *Digitised Optical Sky Surveys* , eds. H.T.MacGillivray and E.B. Thomson, Kluwer Academic Publishers, Dordrecht, p.23.

Seidel, L., 1856, Astronomische Nachrichten, **43**, Nos. 1027,1028,1029.

Sekiguchi, M., Iwashita, H., Doi, M., Kashikawa, N., & Okamura, S., 1992, *Publ. astr. Soc.*

*Pacific,* **104**, 744.

Smart, W.M., 1956, *Spherical Astronomy*, CUP, Cambridge.

Stetson, P.B., 1987, *Publ. astr. Soc. Pacific,* **99**, 191.

Stobie, R.S., 1980, *Journal British Interplanetary Society*, **33**, 323.

Stubbs, C.W., *et al.* , 1994, in *Charge Coupled Devices and Solid State Optical Sensors III*, Proc. SPIE, 1900.

Thejll, P., & Shipman, H.L., 1988, *Publ. astr. Soc. Pacific,* , **100**, 398.

Tulloch, S., 1995, *ING La Palma Technical Note No. 99.*

Tukey, J.W., 1971, .....

Tyson, J.A., & Jarvis, J.F., 1979, *Astrophys. J.,* **230**, L153.

Tyson, J.A., Bernstein, G.M., Blouke, M.M., & Lee, R.W., 1993, in *High-Resolution Sensors and Hybrid Systems*, Proc. SPIE, 1656, 400.

Willstrop, R.V., 1985, *Mon. Not. R. astr. Soc.,* **216**, 411.

Woodward,.....& Davies,.... 1958.....

York, D., *et al.* , 1993, A Digital Sky Survey of the Northern Galactic Cap, NSF proposal.